2012

MEMBRANE IMMOBILIZED REACTIVE Fe/Pd NANOPARTICLES: MODELING AND TCE DEGRADATION RESULTS

Ruo He

University of Kentucky, ranitahe@gmail.com

STUDENT AGREEMENT:

I represent that my thesis or dissertation and abstract are my original work. Proper attribution has been given to all outside sources. I understand that I am solely responsible for obtaining any needed copyright permissions. I have obtained and attached hereto needed written permission statements(s) from the owner(s) of each third-party copyrighted matter to be included in my work, allowing electronic distribution (if such use is not permitted by the fair use doctrine).

I hereby grant to The University of Kentucky and its agents the non-exclusive license to archive and make accessible my work in whole or in part in all forms of media, now or hereafter known. I agree that the document mentioned above may be made available immediately for worldwide access unless a preapproved embargo applies.

I retain all other ownership rights to the copyright of my work. I also retain the right to use in future works (such as articles or books) all or part of my work. I understand that I am free to register the copyright to my work.

REVIEW, APPROVAL AND ACCEPTANCE

The document mentioned above has been reviewed and accepted by the student's advisor, on behalf of the advisory committee, and by the Director of Graduate Studies (DGS), on behalf of the program; we verify that this is the final, approved version of the student's dissertation including all changes required by the advisory committee. The undersigned agree to abide by the statements above.

<div align="right">

Ruo He, Student

Dr. Dibakar Bhattacharyya, Major Professor

Dr. Stephen E. Rankin, Director of Graduate Studies

</div>

MEMBRANE IMMOBILIZED REACTIVE Fe/Pd NANOPARTICLES: MODELING
AND TCE DEGRADATION RESULTS

_____

THESIS

_____

A thesis submitted in partial fulfillment of the
requirements for the Master of Science in Chemical Engineering in the
College of Engineering
At the University of Kentucky

By
Ruo He

Lexington, Kentucky

Director: Dr. Dibakar Bhattacharyya, Alumni Professor of Chemical Engineering

Lexington, Kentucky

2012

ABSTRACT OF THESIS

MEMBRANE IMMOBILIZED REACTIVE Fe/Pd NANOPARTICLES:

MODELING AND TCE DEGRADATION RESULTS

Detoxification of chlorinated organic compound is an important and urgent issue in water remediation nowadays. Trichloroethylene (TCE), as a model compound in this study, has been proved to be degraded effectively by bimetallic nanoparticles (NPs) in solution phase. In this study, Fe/Pd bimetallic NPs were synthesized in poly (acrylic acid) (PAA) functionalized polyvinylidene fluoride (PVDF) microfiltration membranes. TCE dechlorination with these bimetallic NPs was conducted under different pH values and different metal loadings to study the role of corrosion on reaction rates.

One-dimensional mathematical model with pseudo first-order reaction kinetic was introduced to discuss the TCE dechlorination profile in membrane system. Reduction reaction in pores is affected by several parameters including NP loading and size, TCE diffusivity, void volume fraction and surface-area-based reaction rates. This model result indicated that modification is needed to correct the reaction rate obtained from bulk solution in order to represent the actual efficiency of NPs on reduction reaction. In addition, TCE dechlorination mainly occurred near NPs' surface. Second part of model indicated that reduction mechanism with TCE adsorption-desorption behavior could be used to discuss dechlorination with a high TCE concentration.

KEYWORDS: TCE, Fe/Pd nanoparticles, dechlorination, pH effect, pseudo first-order reaction kinetic.

Ruo He

MEMBRANE IMMOBILIZED REACTIVE Fe/Pd NANOPARTICLES: MODELING
AND TCE DEGRADATION RESUTS

By

Ruo He

Dibakar Bhattacharyya

Director of Thesis

Stephen E. Rankin

Director of Graduate Studies

Date

Acknowledgements

First of all, I want to give my biggest thanks to Prof. Dibakar Bhattacharyya for his support and guidance during the past two years. He is first one person that I have never met with such unending passion and dedication about the work he loves. His patience, talent and knowledge have always been helping and guiding me to find the real interests of my life. I will never forget the time that we spent in the office to talk about academic problem which turned out to be this thesis. Not only for academic area, Prof. Bhattacharyya showed his consideration for my life as well when I got lost along the road. I also want to thank his wife Gale, a graceful and noble lady who is always caring about me and making me feel like I am one of her family.

I also deeply appreciate all members in Prof. Bhattacharyya's group whom I worked with: Li Xiao, Minghui Gui, Dr. Vasile Smuleac, Noah Meeks, Scott Lewis, Andrew Tomaino, and Sebastián Hernández for their help and helpful suggestion on my each step of way. I want to specially thank Li Xiao and Minghui Gui, they are not only my dearest labmates, but also good friends to me in my everyday life. I also want to give my appreciation to my friends in University of Kentucky, Xu Jiang, Wei Wen, Binghui Wang, Yushi Meng, Srivenu Seelam, thank you all for making me feel happy and less homesick when I am thousands miles away from my hometown.

Finally, I'd like to thank the most important people in my life, my parents. They raised me up and make me become who I am today. Their endless love and support keep me holding on when I faced challenge and difficulties. Also, my thanks and love to my dear brother, thank you for making me less worried when you choose to stay near to our

parents and take care of them. There's no doubt that my husband, Shiwen Zhao, is the person I want to send my greatest gratitude to. Without your emotional support, I will never come this far. I thank god for bringing you to me to complete my life. I promise that I will always care and love you like you always do to me.

Thank all the people who have ever helped me out and supported me.

Table of Contents

List of Tables

List of Figures

Chaper 1   Introduction

Chlorinated organic compounds have serious issues in water purification and remediation. Trichloroethylene (TCE), one of chlorinated compounds, was an important solvent in manufacturing industry for its excellent greasing effect. However, TCE in ground water could cause serious health issues and even death. It's important to degrade TCE during the water treatment before processing it into public use.

TCE could be degraded in reductive pathway and oxidative pathway. Both pathways have been extensively studied for water remediation in the last two decades (Tyre et al., 1991; Tratnyek et al., 1997; Lin and Gurol, 1998; Smidt and de Vos, 2004; Yeh et al., 2004; Smuleac et al., 2011; Gui et al., 2012). In oxidative dechlorination, oxidative agent such as H_2O_2 was added to solution containing TCE to produce hydroxyl radical that could further dechlorinate TCE. However, the products of this pathway contain not only Cl^- and ethane, but also some chlorinated acid and toxic intermediates formed during the process (Tartakovsky et al., 2003; Qiang et al., 2008; Su et al., 2012).

In reductive way, zero-valent Fe is made by adding highly reductive agent to ferrous or ferric solution, and usually secondary metal or carbon material, such as Ni (Qiang et al., 2008), Cu (Zhu et al., 2010), Cu/C (Zhang et al., 2012), Fe/C (Mackenzie et al., 2012; Swift et al., 2012), Au , Pd (Wang et al., 2012)(Xu and Bhattacharyya, 2008) and Pd/Al_2O_3 (Li et al., 2012), is introduced to form bimetallic system which has high efficiency in TCE dechlorination. However, bimetallic system tends to form clusters or aggregates in solution phase. As a result, its dechlorination activity is reduced because of the decreasing active surface area. There exist several methods to solve the problem by

modifying the synthesis of bimetallic system, including additives controlled seed mediated synthesis (Lu et al., 2007), chemical modification (Ulbricht and Yang, 2005), polymerization (Geismann and Ulbricht, 2005) (Zhao et al., 2009), and layer-by-layer assembly (Datta et al., 2008) methods. However, recently more efficient ways to immobilize bimetallic system is adding support or substrates to decrease the mobility or totally immobilize NPs, including growing nanoparticles on CMC in solution phase (He et al., 2007), coating metal with protective layer (Zhao et al., 2009), membrane immobilization (Xu et al., 2005)(Xu and Bhattacharyya, 2008) and in other porous material (Ruhl et al., 2012). Membrane-immobilized Fe system received extensive attention because of the unique properties of membrane. Membrane has the advantage of large pore size and open structure that could immobilize NPs by chemical treatments; also its large surface area could achieve high sites accessibility to ensure efficient TCE dechlorination.

TCE dechlorination by using iron as a basic reactant has been studied widely these years. Starting from zero-valent Fe particles (Burris et al., 1995) to the introduction of bimetallic system (Liu et al., 2005), first-order reaction rate of TCE degradation has been increased in solution phase at room temperature (298K). Also, dechlorination mechanism (Liu et al., 2005)(Tee et al., 2009)(Andersin et al., 2012) has been developed in different systems as well, generally involving galvanic corrosion observed by Schrick et al. (2002). Although TCE degradation under different conditions such as temperature, pH, metal loading has been extensively studied, the basic reaction mechanism of TCE degradation hasn't been fully understood.

Chaper 2   Objectives

The objectives of this study are to synthesize Fe/Pd functionalized PAA/PVDF membranes, to investigate the TCE dechlorination by applying this membrane system in different conditions, including pH effect and Fe/Pd bimetallic loadings. One-dimensional mathematical model with Thiele modulus was developed to study the TCE concentration profile within membrane and membrane usage as well. Also, TCE dechlorination with adsorption-desorption behavior on membrane surface was discussed to investigate reductive dechlorination mechanism. In order to achieve the overall objective, specific goals need to be achieved including:

(1) to synthesize Fe/Pd immobilized PAA/PVDF membranes by in-situ polymerization, ion exchange and dip-coating;

(2) to investigate TCE dechlorination at different pH values and different metal loadings;

(3) to introduce Thiele modulus and other parameters to discuss the mathematical model by applying pseudo first-order kinetics for TCE dechlorination;

(4) to discuss reaction mechanism of TCE dechlorination considering TCE's adsorption and desorption on the surface of membrane imbedded with Fe/Pd NPs.

Chaper 3   Literature review

In this chapter, it starts with introduction of TCE dechlorination in oxidative way and reductive way. Different mechanisms of both pathways are discussed. Next, two approaches of nanoparticle synthesis including top-down and bottom-up are presented by introducing corresponding techniques, methods and drawbacks applied in synthesizing different materials. Backgrounds and theories of different membrane separations are discussed and functionalized membranes are emphasized because of its versatile properties. It emphasizes the advantages of synthesizing bimetallic NPs in platform or stabilizer in terms of effective reaction, less metal loss and high reaction activity.

3.1 TCE dechlorination pathways and mechanism

TCE degradation in solution phase could be approached in two different pathways, oxidative pathway and reductive pathway. Oxidative pathway achieves TCE degradation mainly by oxdative radicals, which it's a time-consuming process with forming intermediates. For reductive pathway, iron corrosion (e.g. electron transfer by ZVI) is the driving force to dechlorinate TCE by forming free hydrogen ion to replace chloride. With second metal's participation, reaction mechanism involves catalytic hydrochlorination involving hydrogen evolution.

3.1.1 Oxidative Pathway

Oxidative pathway focuses in forming oxidative agent (e.g. OH· from Fenton reaction) in solution to destroy TCE structure by adding high active oxidant. Hydrogen peroxide is widely used in PCE and TCE degradation by Fenton reaction for its cheap price and easy access. Haber and Weiss were the first to propose the hydroxyl radical mechanism of Fenton's reaction. Generally, Fenton reactions take place at low pH to

prevent forming $Fe(OH)_3$ precipitation. However, operation with neutral pH environment is preferred and practical in water remediation. Research has been studied by adding different chelating agents to form Fe^{2+}/Fe^{3+} chelate, in this way, Fenton reaction could be carried out at neutral pH and suppressing ferric oxide from precipitates. Chelating agent such as EDTA, NTA (nitrylotriacetic), DTPA (penta acetic acid), oxalate and citrate were studied and investigated about the effect in suppressing ferric ion's precipitation (Lewis et al., 2009a)(Li et al., 2007).

However, oxidative dechlorination by Fenton reaction is not efficient enough comparing to reductive treatment, and toxic intermediates were formed during the dechlorination. Usually H_2O_2 is coupled with UV, ozone to achieve higher oxidation activity. These oxidation methods by using H_2O_2/UV, H_2O_2/ozone, UV/ozone are known as advanced oxidation process (AOPs) and comparison has been studied (Pignatello et al., 2006)(Ried and Krüger, 2009). Still, intermediates remediation is the biggest issue using oxidative pathway for TCE dechlorination.

3.1.2 Reductive Pathway

TCE was reported to be dechlorinated in solution phase by using zero-valent metal or bimetallic system since Gillham and O'Hannesin proposed that metallic iron fillings could be used for an in situ, passive groundwater remediation(Roberts et al., 1996; Tratnyek et al., 1997; Hara et al., 2005). Zero-valent iron was firstly studied and reported to decay chlorinated compounds in solution at different pH values with different particle sizes. Larger size of iron particles (obtained from commercial access with 20-50 μm) have been reported to dechlorinate TCE (Hara et al., 2005). It took 500 hr to degrade 80% of TCE while forming intermediates in solution by adding 100 mg Fe powder in 10ml

100 mg L^{-1} TCE solution. Afterwards, Wang and Zhang in Lehigh University developed a method to synthesis iron nanoparticles focusing on environmental remediation in solution phase (Wang and Zhang, 1997; Zhang, 2003). By using highly reductive agent $NaBH_4$, Fe^{3+} is reduced to form ZVI in solution phase:

$$4Fe^{3+} + 3BH_4^- + 9H_2O \rightarrow 4Fe^0 \downarrow + 3H_2BO_3^- + 12H^+ + 6H_2 \qquad \text{(E3.1)}$$
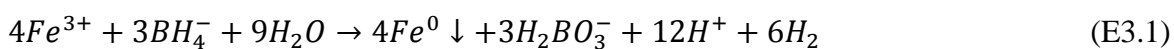
Recently, bimetallic NPs stand out for its fast reaction in TCE dechlorination. Synthesis and reaction of different second metals have been extensively studied. The participation of second metal not only accelerates dechlorination rate, but also suppresses toxic intermediates' formation.

TCE dechlorination has been extensively studied and investigated. Mechanisms are different by applying iron particle or bimetallic system. For dechlorination by iron particles (including iron powder and iron NPs), direct electron transfer contributes to TCE decay. In the case of bimetallic system, catalytic reaction is performed.

One acceptable mechanism for dechlorination of chlorinated organic compounds by ZV metal was developed by Roberts in 1996. In Figure 3.1, He explained the two pathways of trans-dichloriethylene, i.e. hydrogenolysis ($RCl + 2e^- + H^+ \rightarrow RH + Cl^-$, one chloride is replaced by one hydrogen) and β-elimination ($RCl=RCl + 2e^- \rightarrow R\equiv R + 2Cl^-$, two chlorides are released). There are also hydrogen addition reactions when ethylene transforms to ethane (Hara et al., 2005). With ZVI's presence, reaction could be described as:

$$Fe^0 \rightarrow Fe^{2+} + 2e^- \qquad \text{(E3.2)}$$
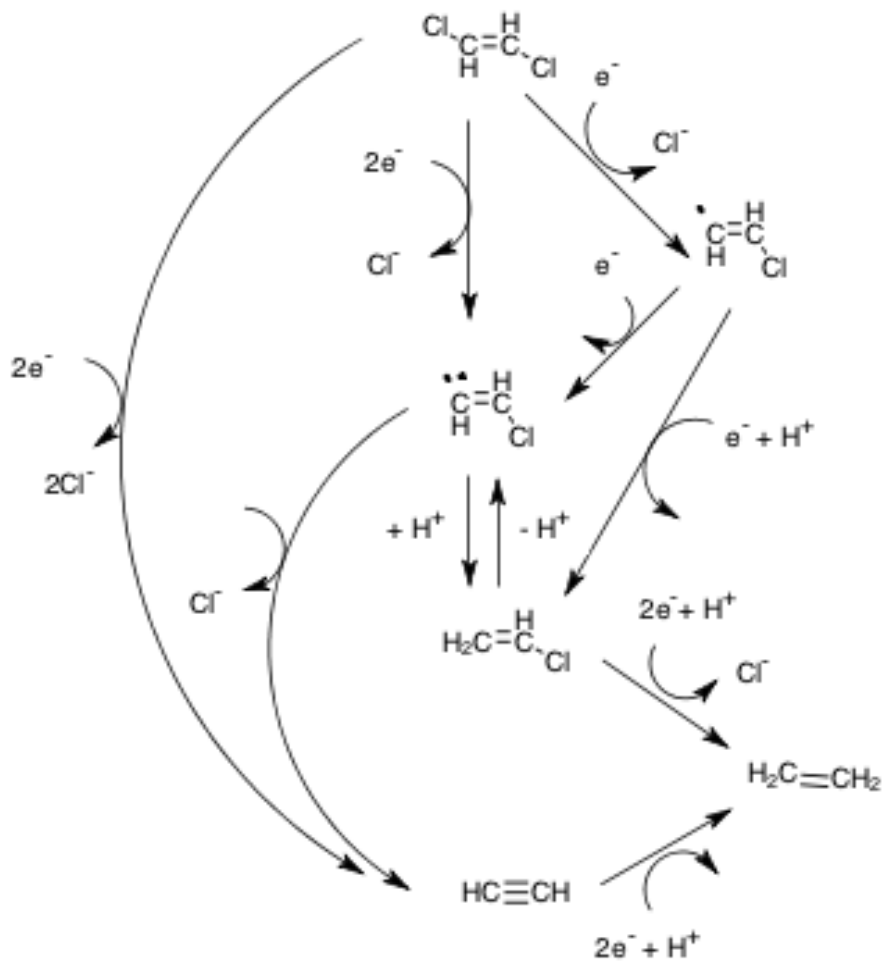
Figure 3.1 Reductive dechlorination pathway of trans-dichloroethylene by ZVI. (Reprinted (adapted) with permission from (Roberts et al., 1996). Copyright (1996) American Chemical Society.)

$$RCl + 2e^- + H^+ \rightarrow RH + Cl^- \tag{E3.3}$$

$$RCl + Fe^0 + H^+ \rightarrow RH + Cl^- + Fe^{2+} \tag{E3.4}$$

One iron's corrosion in water provides 2 electrons which further dechlorinate RCl to form 1 ferrous ion and 1 chloride ion. Without any other materials' participation or any methods' assistance, it takes days to complete dechlorination process.

By adding second metal to ZVI dechlorination system, reaction mechanism is no longer simply electron transfer, but catalytic hydrochlorination. Usually, second metal particles act as catalyst to promote chloride formation. Bimetallic system such as Fe/Pd (Xu and Bhattacharyya, 2008; Wang et al., 2012), Ni/Fe (Qiang et al., 2008; Tee et al., 2009), Al_2O_3/Fe (Li et al., 2012), have been studied widely for the last 20 years, degradation rate of chlorinated compounds has been dramatically increased by one or two orders of magnitude. Surface-area-normalized reaction rate k_{SA} was investigated in solution phase applying different metal system, including Fe powder, Fe/Pd powder, Fe NPs and Fe/Pd NPs (Wang and Zhang, 1997). The k_{SA} value for Fe/Pd NPs treatment was 0.1 L h^{-1} m^{-2}, and 3.0×10^{-3} L h^{-1} m^{-2} for Fe NPs treatment. Reaction rate increased by 200 times.

Even though different approaches of bimetallic TCE dechlorination have been developed, the mechanism of second metal's function and participation has not been fully understood and studied. However, mechanism of TCE dechlorination by using CMC-stabilized Fe/Pd NPs was proposed by considering Fe corrosion in water and hydrogen

formation on the surface of NPs. The corresponding reactions are listed below (Cwiertny et al., 2006; He and Zhao, 2008):

$$Fe^0 + 2H_2O \rightarrow Fe^{2+} + H_2 + 2OH^- \tag{E3.5}$$

$$Fe^0 + 2H_2O \xrightarrow{Pd} Fe^{2+} + H_2 + 2OH^- \tag{E3.6}$$

$$H_2 \xrightarrow{Pd} 2H \cdot \tag{E3.7}$$

$$TCE + 8H \cdot \rightarrow ethane + 3H^+ + Cl^- \tag{E3.8}$$
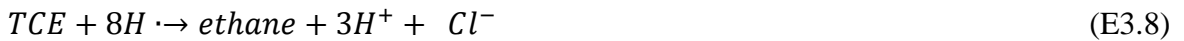
Since water is one of reactants in this system, and proton from solution converts to hydrogen atom near the surface of iron particles, one could expect that no reaction, i.e. no TCE is dechlorinated when Fe particles are fully covered by second metal. The study of different coverage of Pd on Au surface in TCE dechlorination showed that observed reaction rate constant dropped when Pd coverage was more than 59.3% (12.3 wt%). Almost no TCE degraded when Au was full with 100% Pd coverage (Nutt et al., 2006).

Oxidative pathway and reductive pathway are both effective in TCE dechlorination. With high reaction rate and suppression of intermediate's formation, reductive pathway is more popular in fields of chlorinated compounds' remediation. However, fundamental mechanism of different reaction system has not been fully illustrated and investigated, as well as the change of NPs' structure, size, formation before and after reaction.

3.2 Synthesis of nanoparticles

Nanotechnology is a technology including design, synthesis, characterization and application of nanoscale materials. Nanostructured materials receive extensive attention because of its supreme properties than bulk materials, such as catalyst activity, thermo stability, mechanical strength, magnetic property, optical property and many others. To study nanostructured material also provides fundamental understanding of its physical property and explanation of chemical phenomena. Different syntheses of nanoparticles are usually classified as top-down and bottom-up.

For top-down synthesis methods, large-scale materials are broken down into lower-level-sized structure (especially for Ag, TiO_2, Si, ZiO, FeO_x and other nanoparticles) by different treatments, including lithography, UV/ozone, laser or plasma. For example, silica nanoparticle pattern was fabricated lithographically over large area by pin-coating, interferometric lithography, and reactive-ion etching (Xia et al., 2007). Precise size of silica nanoparticles with diameter 15-50nm were successfully formed and layered in different patterns. Recently, iron oxide (FeO_x) was reported to be synthesized via a top-down physical technique consisting in Laser Ablation Synthesis in Solution (LASiS) forming nanoparticles size from 20nm-100nm(Amendola et al., 2011). Without adding chemicals and stabilizers, FeO_x NPs were synthesized directly in solution phase and performing good magnetic property. However, nanoparticles made by top-down approach might have some drawbacks such as imperfection of NPs' surface, broad distribution of NPs' sizes and others. The biggest problem is surface's imperfection and defects that usually occurred by using lithographical approach. Defects on the surface could have an

10

impact on chemical and physical performance, as well as catalytic activity decay(Behari, 2010).

More attentions are paid to bottom-up approach in recent studies. Nanoparticles are fabricated atom by atom, molecule by molecule forming more identical NP size with identical physical and chemical properties. Different methods include sol-gel process(Chen and He, 2001)(Lu et al., 2002), chemical vapor deposition (CVD)(Li et al., 2001)(Durrer et al., 2008), self-assembly(Boal et al., 2000)(Grzelczak et al., 2010), microwave synthesis(Seol et al., 2011), template synthesis(Xu et al., 2005) and other methods. The advantages of using bottom-up approach are less defected surface, homogeneous distribution and more uniform size and shape distribution. For example, carbon nanotubes are widely studied and usually fabricated by CVD, sometimes PECVD (plasma enhanced CVD). It was reported that C_2H_4 or CH_4 as the source of carbon, decomposed in an anaerobic environment with catalyst at temperature 600-900 ^{o}C, forming CNT with diameter ranging 15-90 nm(Jung et al., 2001). In solution phase, Ag, Au, Fe, Pd, Ni, and alloy were synthesized generally by reducing its corresponding ion. For example, Fe nanoparticles were synthesized by reducing Fe^{2+} or Fe^{3+} in solution with sodium borohydride ($NaBH_4$)(Glavee et al., 1995). However, NPs with magnetic property tends to form aggregates and clusters in solution to decrease its surface area as well as catalytic activity.

3.3 Nanoparticles in functionalized membranes

Membrane separation has been used widely not only in lab level but also industry scale for many areas, such as water remediation, gas separation and biomedical applications. In general, membrane separation could be classified into four groups

according to different separation approaches: (1) pressure driven including reverse osmosis (RO), nanofiltration (NF), ultrafiltration (UF), microfiltration (MF) and membrane bioreactors; (2) thermal driven, as membrane distillation; (3) osmosis driven, as forward osmosis; (4) charge driven, as electrodialysis. Among all different approaches, pressure driven membrane separations are most popular and extensively applied in water purification and industrial water remediation. However, separation only involves physical behaviors, such as sieving of different particle sizes, diffusion caused by concentration difference, and ion exchange. Functionalized membrane could provide open sites to chemical groups, polymeric groups, and other materials. Also, it could achieve specific separation for certain materials and reaction. Different methods have been reported in synthesizing functionalized membrane including layer-by-layer assembly (Smuleac et al., 2006)(Datta et al., 2008), polymerization (Geismann and Ulbricht, 2005)(Ulbricht and Yang, 2005) and others.

Nanoparticle functionalized membrane has been studied due to its promising properties including preventing nanoparticles forming aggregates, performing high chemical stability and effective reaction capability. In nanoparticle/membrane system, not only nanoparticles achieve homogeneous distribution, but also membrane property could be enhanced. For example, it's reported that in TiO_2/PVDF membrane prepared by phase inversion method, the smaller nanoparticles (~10 nm diameter) could improve the antifouling property of the PVDF membrane more remarkably (Cao et al., 2006).

However, what's more attractive in nanoparticle/membrane is its application in various areas such as heavy metal removal (Bhattacharyya et al., 1998)(Hota et al., 2008), gas separation (Ahn et al., 2008)(Hu et al., 2007), and degradation of toxic organic

compounds (Xu and Bhattacharyya, 2007)(Wang et al., 2008)(Tee et al., 2009)(Gui et al., 2012). Recently, bimetallic functionalized membrane was studied in water remediation area. Zero-valent iron (ZVI) were reported to effectively to destroy chlorinated compounds in solution phase but produce toxic intermediates. By coating a second metal (Ni, Pd, Cu) on the surface of ZVI nanoparticles, reaction rate increased by 1-2 magnitude. However, nanoparticles' mobility in solution caused issues such as metal loss, aggregation. By synthesizing nanoparticles in a platform or a stabilizer, such as functionalized membrane, it is reported that no intermediates formed, less particles aggregated and effective degradation during the reaction (Smuleac et al., 2010)(Xu et al., 2005).

Chaper 4   Experimental Section

4.1 Introduction

This chapter includes description of all the materials needed in experiments, also procedure of all measurements and model set-ups. In addition, synthesis of PAA in situ polymerization, ion exchange for Fe^{2+}, Pd coating and diffusion experiments will be discussed in details. The PVDF membranes and Fe/Pd NPs functionalized membranes were characterized by scanning electron microscopy (SEM). TCE dechlorination was determined by using gas chromatography equipped with mass spectrometry (GC/MS), and Cl^- concentration after reaction was measured by Accumet combination chloride electrode. The analysis equipment applied for Fe and Pd NPs' loading and loss was atomic adsorption (AA). Assumptions were made to simplify the expression to describe TCE dechlorination within membrane pores, TCE's adsorption-desorption was taken into consideration as well.

4.2 Materials

Trichloroethylene (TCE = 99.9+ %), ferrous chloride (FeCl$_2$ 4H$_2$O), sodium hydroxide (NaOH) solution, sulfuric acid (H$_2$SO$_4$) solution, nitric acid, hexane (GC-MS grade) were purchased from Fisher Scientific. Potassium persulfate (K$_2$S$_2$O$_8$ = 90+ %) was purchased from EM Science. Acrylic acid (CH$_2$=CHCO$_2$H = 99%), potassium tetrachloropalladate (II) (K$_2$PdCl$_4$ = 98%), sodium borohydride (NaBH$_4$ = 99.99%) were purchased from Sigma-Aldrich and ethylene glycol (EG) from Mallinckrodt.

Hydrophilized polyvinylidene fluoride (PVDF) microfiltration membranes with the nominal pore size of 650 nm and thickness of 125 μm were purchased from Millipore Corporation.

Chloride reference solution (certified as 1000 mg L^{-1}) was purchased from Thermo Electron Corporation. Iron reference solution (certified as 1000 mg L^{-1}), palladium reference solution (certified as 1000 mg L^{-1}) and deionized ultrafiltered (D.I.U.F.) water were obtained from Fisher Scientific. All chemicals were of reagent grade.

4.3   Methods

4.3.1   PAA Polymerization on PVDF Membranes

The method used in this paper to polymerize acrylic acid (AA) in PVDF membranes was in-situ polymerization (Xu et al., 2005). The polymerization solution was composed of 1ml EG (cross-linked), 20ml acrylic acid (monomer) and 1 wt% potassium persulfate (initiator). The composition ensured 10:1 molar ratio of acrylic acid to EG. Each mole of EG would bind two moles acrylic acid in order to avoid the lost and mobilization of AA in the membrane. PVDF membrane was soaked in the polymerization solution for 5min and was firstly sandwiched between two sheets of polyethylene, then two glass plates. In this way, excessive acrylic acid was suppressed to polymerize on the PVDF membrane surface, also preventing excessive PAA formation within the pores. Acrylic acid was polymerized at 90 $^{\circ}$C for 4 hours with continuous nitrogen gas to prevent the contact with oxygen, which acts as an initiator for the polymerization reaction.

15

4.3.2 Fe and Fe/Pd Bimetallic Nanoparticles Synthesis in PAA/PVDF Membrane

The flowchart for membrane functionalization and NPs synthesis is shown as Figure 4.1. Prior to ferrous ion exchange, PAA functionalized membranes were immersed in NaCl (10-20 wt%)/NaOH solution at pH 7-9 (adjusted with 0.1 mmole L^{-1} NaOH) for 12 hours to convert the $-COO^-H^+$ to $-COO^-Na^+$ form. The purpose was to minimize the pH effects on ion exchange equilibrium, thus enhancing the ion exchange capacity. In the next step, the membrane was washed with D.I.U.F. until the pH of the washing solution became neutral. Then, the membrane was immersed in 200 ml $FeCl_2$ solution (typically 180 mg L^{-1} Fe^{2+}) at pH 4-6 for 4 hours. Nitrogen was purged continuously to minimized Fe^{2+} oxidation. The reduction with $NaBH_4$ ensured Fe NPs' formation. If Fe loading tested by AA was relatively low ($\leq$ 4mg on PAA/PVDF membrane with 13.2 cm^2 area) and second ion exchange for Fe^{2+} is necessary to be operated. Fe functionalized PAA/PVDF membrane was immersed in the Na^+ solution for another 12 hours and then reacted with Fe^{2+} for another 4 hours. The secondary metal, Pd, was deposited on the Fe NPs by immersing the membrane (typically for 12 hours) in a K_2PdCl_4 solution containing ethanol/D.I.U.F. (90:10 vol% mixtures), preventing the oxidation of the highly reactive Fe NPs. The amount of K_2PdCl_4 added was calculated basis on the desired amount of Pd and the previous Fe loading, and it was expressed in wt% with respect to the amount of Fe. The deposition occurred via the well-known redox reaction:

$$Pd^{2+} + Fe^0 \rightarrow Pd^0 + Fe^{2+} \tag{E4.1}$$

The Fe/Pd modified PAA/PVDF membrane was stored in ethanol until the use for dechlorination experiments. Batch mode experiment was performed using TCE in order to determine the reactivity of the immobilized Fe/Pd NPs.

PVDF membrane
(650nm pore diameter)

In situ polymerization

PVDF-PAA membrane

FeCl$_2$
Ion exchange

PVDF-PAA-Fe^{2+} membrane

In situ polymerization at 90 °C for 4 hr:
AA - acrylic acid
EG - ethylene glycol, cross-linking agent
KPS - potassium persulfate, initiator
PAA - polyacrylic acid
PVFD - polyvinilidene fluoride

NaBH$_4$
Fe^{2+}→Fe^0

Pd

Fe^0

K$_2$PdCl$_4$

PVDF-PAA-Fe/Pd membrane

PVDF-PAA-Fe^0 membrane

Figure 4.1 Schematic for PAA coating and Fe/Pd nanoparticle synthesis in PVDF membrane.

4.3.3 Measurement of TCE diffusion coefficient through deactivated Fe/Pd PAA/PVDF membranes

The Fe/Pd modified PAA/PVDF membrane was placed in D.I.U.F. water with open lid for 48 hours, reacting with oxygen to completely deactivate Fe/Pd NPs. Then membrane was immobilized between the two compartments of a stainless-steel diffusion cell, with area of 3.5 cm^2. One compartment was filled with 250 ml feed solution with 30 mg L^{-1} TCE (pH ~ 6.5); the other was filled with same amount of D.I.U.F. water to serve as the permeation compartment. Both compartments were well mixed during diffusion experiment by placing stirring rods inside the compartments, and magnetic field was applied. Two ml solution of both sides were drawn from both compartments at different time and were extracted by pentane (EDB was added as internal standard) for 40 min. TCE concentration was measured by GC-MS. The following equation developed by Yang et al. (Lape et al., 2002) was used to determine the diffusion and partitioning coefficient of TCE in PAA/PVDF membrane.

$$\frac{C_P}{C_F} = \left[\frac{D_m H}{L} \left(\frac{A}{V_c} \right) \right] \left(t - \frac{L^2}{6D_m} \right) \tag{E4.2}$$

where C_F and C_P is the concentration in feed side compartment and permeate side compartment respectively. L is the membrane thickness (m), A is the permeate membrane area (m^2), V_c is the volume of both feed and permeate sides (m^3), t is the permeate time (s). H is the TCE partitioning coefficient through membrane, D_m is the TCE diffusivity through the membrane (m^2 s^{-1}). Because C_P is much less than C_F during the experiment, we assumed that the change of C_F is negligible and remains constant.

The result for TCE diffusion through deactivated Fe/Pd modified PAA/PVDF membrane was shown in Figure 4.2. The figure stated that TCE concentration in permeate side compartment is proportional to time. Using equation E4.2 to fit the data, H was calculated to be 6.85, and D_m was 6.50×10^{-12} m^2 s^{-1} for TCE diffusion through PAA/PVDF membrane with deactivated Fe/Pd NPs at 10 ± 0.2 ^{o}C with pH 6.5. H and D_m were respectively 2.74 and 3.25×10^{-11} m^2 s^{-1} for TCE diffusion through PVDF membrane. Value of partitioning coefficient indicated that PAA has better swelling property and more TCE was restrained in PAA layer, comparing to the result by using PVDF membrane. Also, PAA polymerization occupied around 43% (discussed in section 6.2), TCE diffusivity in functionalized PAA/PVDF membrane was expected be lower than that in PVDF membrane with open pores.

Considering the volatility of TCE, experiment was conducted at 10 ± 0.2 ^{o}C (283 ± 0.2 K). Diffusivity used in model and later in calculation would be corrected by Wilke-Chang equation, which stated that the correlation between temperature and diffusivity follows the rules:

$$\frac{D_{m1}}{D_{m2}} \mu \frac{T_1}{T_2} \qquad (E4.3)$$

Therefore, the calculation shows that at room temperature (298 K), TCE diffusivity was 6.84×10^{-12} m^2 s^{-1}.
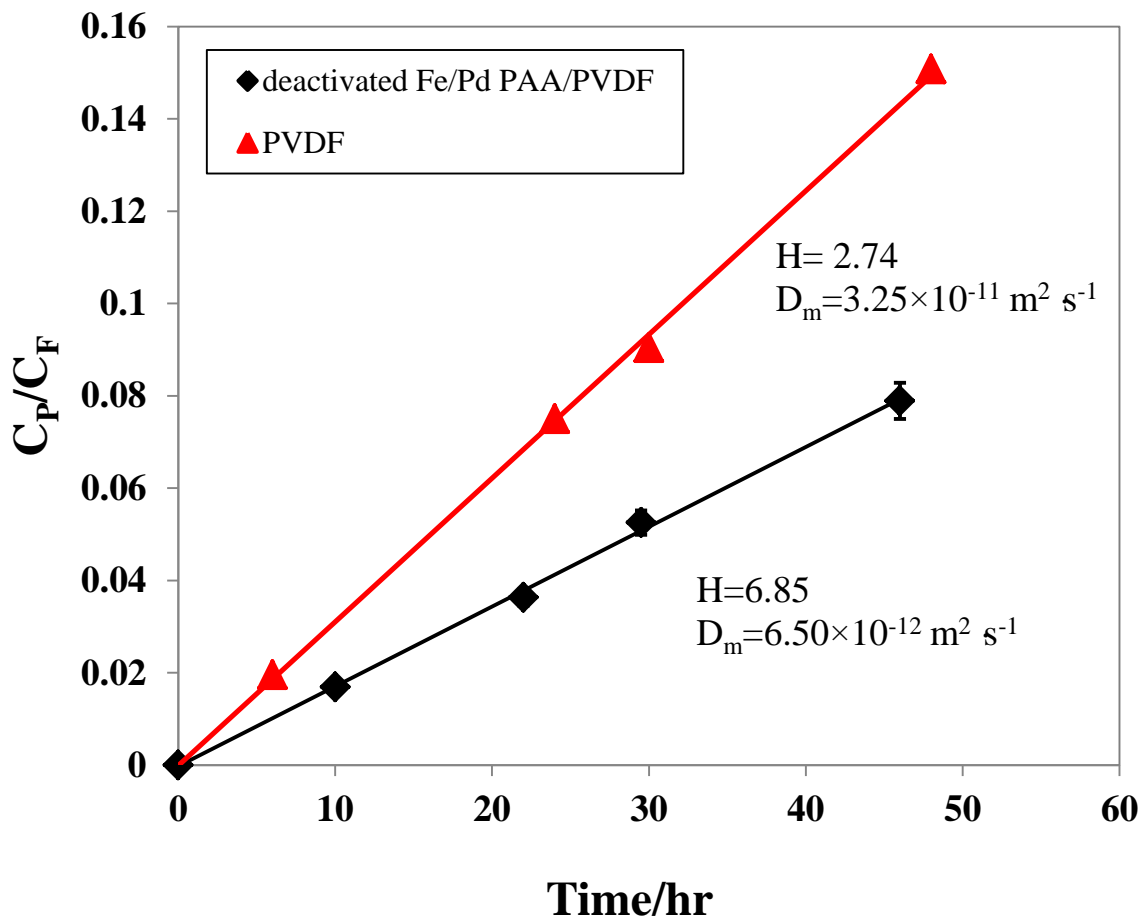
Figure 4.2 Experiment of TCE diffusion through deactivated Fe/Pd modified PAA/PVDF

membrane at 10 ± 0.2 ^{o}C with pH 6.5. (Membrane area: 3.5 cm^3; membrane thickness: 125

µm; compartment volume: 250 mL)

4.3.4 Characterization of Membrane and Fe/Pd nanoparticles

Hitachi S-3200 SEM was applied to observe metal NPs embedded on the surface and inside the PAA/PVDF membranes. For functionalized Fe/Pd PAA/PVDF membrane, particle size and distribution were characterized by SEM. Blank PVDF was also observed to the contrast of the sample after functionalization.

4.3.5 Fe/Pd Bimetallic Nanoparticles Synthesis in solution phase with/without CMC

The method of preparing Fe/Pd bimetallic NPs in solution phase with the presence of CMC was published in He's work (He et al., 2007). In this study, solution containing 0.5 wt% CMC was prepared for metal coating. $FeCl_2$ $4H_2O$ was added to the deoxidized D.I.U.F. water to prepare Fe^{2+} solution. Concentration of Fe applied in this study is 0.25 g L^{-1}. Fe^{2+} was then reduced by adding $NaBH_4$ (BH_4/ Fe^{2+} = 2.5) to the solution. K_2PdCl_6 was used as the source of Pd NPs, the concentration applied was 1 wt% and 5 wt% (based on Fe loading) for comparison with the membrane system. All NPs were prepared right before TCE degradation experiments to ensure its high reaction activity.

The CMC-stabilized Fe/Pd particle size was determined by dynamic light scattering (DLS, DelsaNano C, Beckman). Fe/Pd NPs were prepared as 0.25 g L^{-1} in 40 ml D.I.U.F. with 0.5 wt% CMC. Fe^{2+} was reduced by adding $NaBH_4$ to the solution. DLS samples were prepared by diluting the solution containing CMC-stabilized Fe/Pd NPs, and were sonicated before tests. In all measurements, triplicate samples of before reaction and after reaction were analyzed.

4.3.6 Metal Analysis

The amount of Pd and Fe captured during ion exchange and lost after reaction (membrane was digested by immersion in 25 vol% HNO_3) were separately quantified by Atomic Absorption Spectroscopy (AAS) using a Varian SpectrAA 220 Fast Sequential atomic absorption spectrometer. For Pd, samples were analyzed at a wavelength of 246.6 nm. The calibration curve was created by using 5 different concentrations of Pd ranging 0.2 and 28 mg L^{-1} Pd with $R^2 = 0.9999$. The error of analysis was $< 1.8\%$ in all cases. For Fe, the lamp was operated at a wavelength of 386.0 nm. The calibration curve was created by using 5 different concentrations of Fe ranging from 25 to 200 mg L^{-1} with $R^2 \geq 0.991$ and average analytical error of 2.8% in all cases.

4.3.7 TCE Dechlorination Analysis

TCE stock solution was prepared before the dechlorination experiments at the pH values ranging from 4 to 10 (typically with 30 mg L^{-1} concentration). TCE Dechlorination was conducted by immerging PAA/PVDF membranes containing Fe/Pd NPs (13.2 cm^2 external area and 125 μm thickness) in 40 ml sealed vials containing TCE solution. Samples were collected with a syringe at different time. TCE samples were extracted in same amount of pentane with 200 mg L^{-1} 1, 2 dibromoethane (EDB) as internal standard, and analyzed with a Hewlett Packard Series II 5890 GC-MS. Sample was injected to GC-MS after 30 min extraction. TCE peak usually came out around 10.43 min and EDB peak at 13.56 min (see Figure 4.3). TCE standard curve was investigated to ensure the accuracy of TCE concentration. Different standard solutions ranging 5 mg L^{-1} to 40 mg L^{-1} were prepared and typical plot of area ration (TCE area/EDB area) to TCE concentration was shown in Figure 4.4. The average analytical error was $< 8.5\%$.
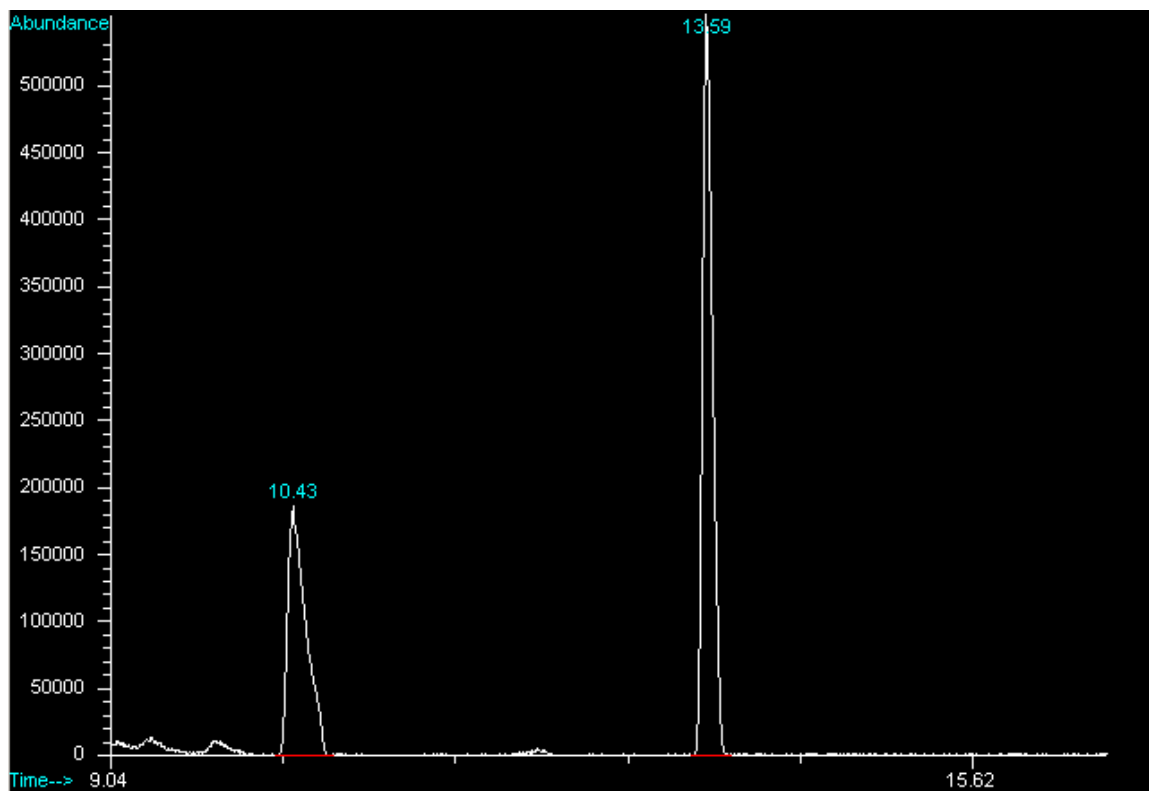
Figure 4.3 Typical TCE and EDB reference spectrum by GC-MS. (TCE concentration in solution: 30mg L^{-1}, internal standard EDB concentration in pentane: 200 mg L^{-1})
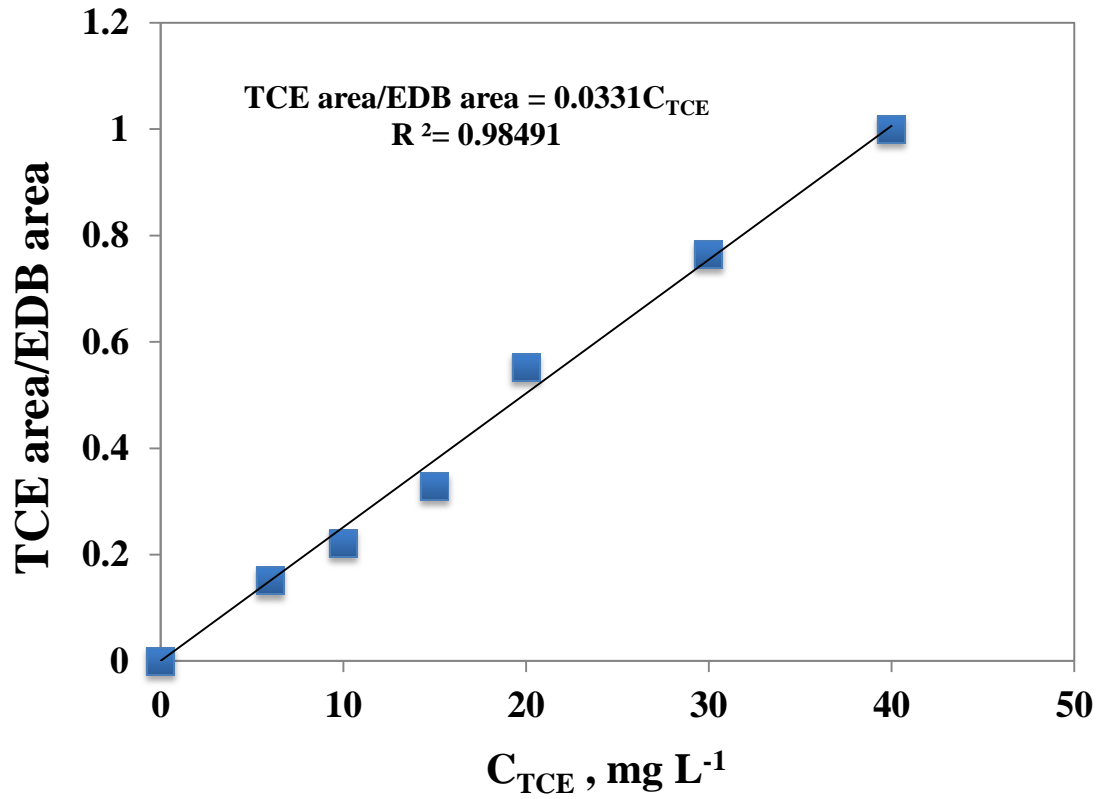
Figure 4.4 Typical TCE concentration standard curve. (Internal standard EDB concentration: 200 mg L^{-1})

4.3.8 Chloride Concentration Analysis

The concentration of Cl⁻ of samples at different time by CMC-stabilized and membrane-immobilized Fe/Pd NPs was measured by using the Accumet combination chloride electrode. Standard 1000 mg L⁻¹ chloride solution was diluted to five different standard concentrations ranging from 1 ppm to 25 ppm, blind standard solution was used to exam the accuracy of calibration curve. 2 vol% of 5 M sodium nitrate internal standard was added to every sample and calibration curves was conducted to measure chloride concentration after every experiment. Random sample was tested by adding same volume of known standard chloride solution to ensure result's accuracy by the change in sample's concentration. Then concentration of TCE consumed in the samples was back calculated based on the assumption of a total dechlorination (1 mole of TCE degraded releases 3 moles of Cl⁻). In this analysis, chlorination concentration in all cases was performed in between 1 and 23 mg L⁻¹. Detecting limitation is 1 mg L⁻¹. R^2 in all calibration curves $\geq$ 0.9865, and the average analytical error was $< 5.6\%$.

Equation E6.4 (Nernst equation) was used to describe the relation between voltage signal and chloride concentration:

$$E = a \times \ln [Cl^-] + b \tag{E4.4}$$

where E is the voltage signal detected by chloride electrode (mV), $[Cl^-]$ is the standard Cl^- concentration. Coefficient a and b are constants. With calibration curve, chloride concentration was obtained by measuring triplicate samples.

One typical chloride calibration curve was shown in Figure 4.5.
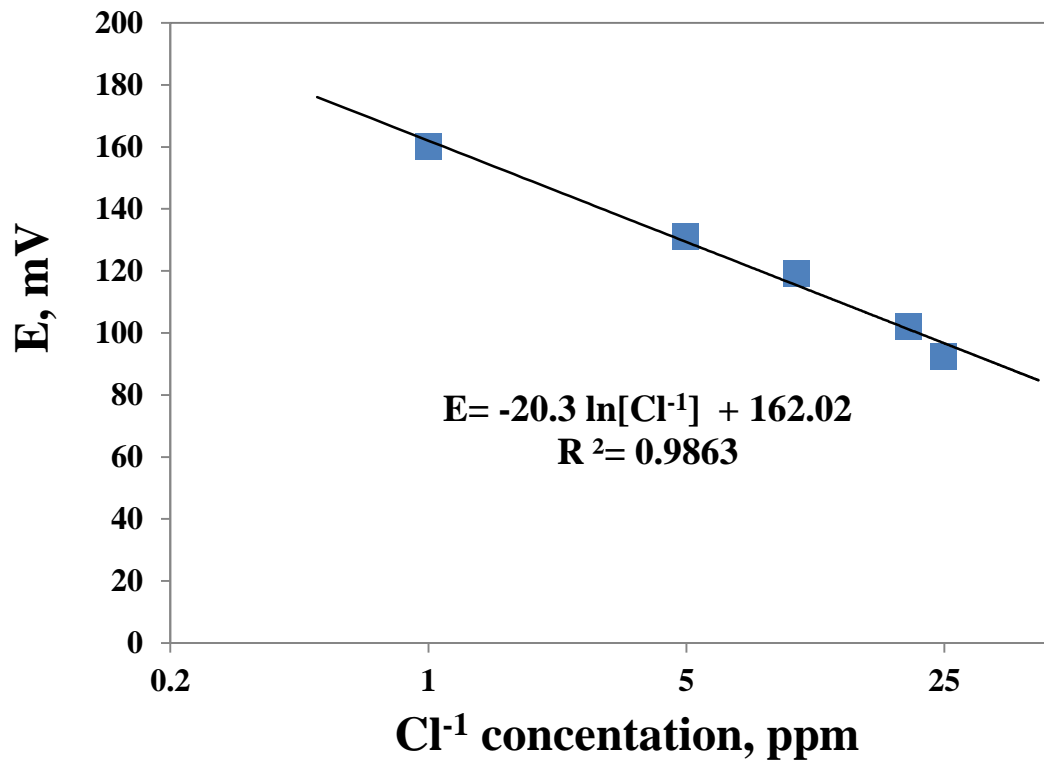
Figure 4.5 Chloride calibration curve by chloride electrode. Different standard solutions were obtained by dilution of 1000 mg L^{-1} standard chloride solution purchased from Thermo Electron Corporation.

Chaper 5　　　Mathematical Modeling Section

Introduction

Membranes with its large open structure and high active sites accessibility not only effectively prevent Fe/Pd NPs from forming aggregates, but also provide NPs the homogeneous distribution on the surface and inside membranes. Extensive studies have been carried out to study the mechanism, dechlorination phenomena of TCE degradation in membrane. However, TCE dechlorination experiments by using functionalized membrane in batch mode only investigated TCE concentration change in solution phase, but the description of the concentration change inside membrane pores has never been studied or reported. Also, TCE's adsorption-desorption behavior might paly a role in reduction mechanism. Its proposed mechanism with adsorption-desorption behavior was discussed.

5.1　TCE dechlorination kinetics models

The discussion of TCE concentration change inside membrane pores is important to imply the effectiveness of membrane. At low concentration, TCE could be completely degraded by Fe/Pd NPs before diffusing through membrane. This indicates that not all the immobilized Fe/Pd NPs on PAA/PVDF membrane are reacted with TCE, thus k_{obs} and k_{SA} value obtained from experiments needs to be modified to present the actual reaction rate. In addition, membrane treatment exists mass transfer resistance; diffusion limiting is expected and could be determined by Thiele modulus. Also, it is found that H_2 is a reactant during dechlorination, its formation mainly occurred near the surface of bimetallic system (He and Zhao, 2008), which means that TCE's adsorption-

27

desorption behavior could play an important role in correcting TCE dechlorination reaction rate expression.

5.1.1 One-dimensional model

In order to discuss TCE concentration change within Fe/Pd functionalized PAA/PVDF membrane, one-dimensional model is developed with acceptable assumptions. Packed bed model is built to simulate the mass transfer and reaction performance of TCE inside membrane (schematic diagram was shown in Figure 5.1). There are several variables involved in the dechlorination reaction, including pH value, bimetallic loading, particle size and void volume fraction.

Fe/Pd functionalized PAA/PVDF membranes use PVDF as a membrane plat form, PAA layer, Fe/Pd NPs are functionalized on membrane surface and in membrane pores. Unmodified PVDF membranes have normalized poresize as 650 nm with 70% porosity, and PAA was calculated to occupy 57% of open structure based 5.7 $\pm$ 0.5 mmole PAA/g dry membrane. Most metal loading was assumed to form in membrane pores, and occupation rate was 1.1% based on 10mg Fe NPs (50 nm d_p) embedded in PVDF membranes with 13.2 cm^2 external area, 125 μm thickness and 70% porosity (1 g of Fe NPs will be needed to fill the whole membrane).
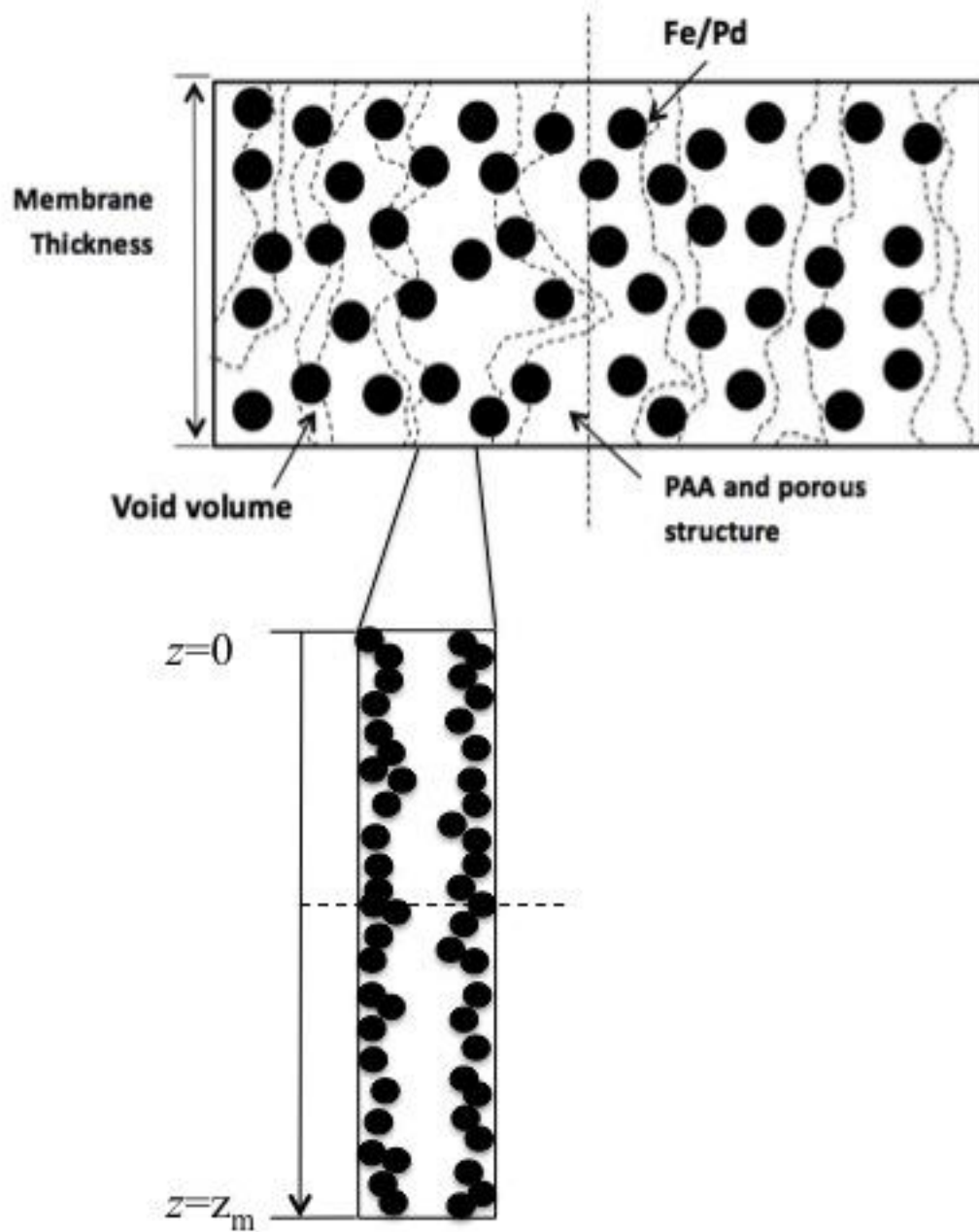
Figure 5.1 Schematic diagram showing the distribution inside the membrane pores.

Firstly, several assumptions are considered to simplify the system for understanding purpose. The following assumptions are accepted to describe the system in batch mode:

- Fe/Pd NPs have homogenous distributions in PAA/PVDF membranes.

- TCE concentration maintains same value on membrane surface.

- Horizontal diffusion through PAA/PVDF layer is negligible considering large ratio of membrane pore length to pore radius.

- Diffusivity of TCE remains same value at different pH.

After applying the assumptions, the following second order ordinary differential equation was gained to describe the system.

$$D_m \frac{d^2 C_A}{dz^2} + r_A = 0 \tag{E5.1}$$

where C_A is the TCE concentration in membrane pores (mmole L^{-1}). D_m is TCE diffusivity through the PAA/PVDF membrane (m^2 s^{-1}). z is the axial direction of membrane. r_A is the rate of generation of TCE per volume, (mmole s^{-1} L^{-1}).

The rate of TCE generation r_A has different expressions depending on its TCE dechlorination types. For example, intermediates' formation perform in solution when TCE is dechlorinated by ZVI, first order reaction considering transformation to other products could be applied (Hara et al., 2005). Also, TCE's adsorption-desorption behavior on NPs' surface played roles in reaction (Burris et al., 1995; Tee et al., 2009). However, pseudo first-order reaction is widely accepted in TCE dechlorination mechanism in reductive pathway (Chen et al., 2001; Xu and Bhattacharyya, 2007; Smuleac et al., 2010). In addition, k_{obs} value obtained from all experiment data only

represents the reaction in solution phase but not reflect the actual reaction mechanism. The reaction rate constant k_m in membrane pores imbedded with NPs has never been reported.

In this model, pseudo first-order reaction is applied and analytical solution could be achieved:

$$r_A = \frac{dC_A}{dt} = -k_m C_A \tag{E5.2}$$

where k_m is the reaction rate constant in membrane (h^{-1}).

In membrane system with NPs, TCE dechlorination occurred on the surface of NPs, which indicates that reaction rates should consider the effect of nanoparticle size, NPs' surface area, NP loading and void volume. The following equation is used to express k_m:

$$k_m = (1\text{-}\varphi)a_s\rho_m\,k'' \tag{E5.3}$$

where k'' is the surface-area-based rate constant (L m^{-2} h^{-1}) (sometimes designated as k_{SA}). φ is the void volume fraction, indicates that TCE flows through membrane without reduction by NPs, and it could be affected by NPs loading, NP size, PAA loading and pH. a_s is the surface area of the NPs (m^2 g^{-1}), 15.24 m^2 g^{-1} based on 50 nm d_p. ρ_m is the mass concentration of the NPs (g L^{-1}), ranging from 0.3 g L^{-1} and 4.4 g L^{-1} based on Pd loading, and membrane pore volume.

By doing dimensionless treatment, this model could be used in any membrane system with different thickness and initial TCE concentration; solution of E5.1 combining E5.2 and E5.3 could be given by following equation:

$$\frac{C_A}{C_{A0}} = C_1 cosh\left(z'z_m\sqrt{\frac{(1-\varphi)a_s\rho_m k''}{D_m}}\right) + C_2 sinh\left(z'z_m\sqrt{\frac{(1-\varphi)a_s\rho_m k''}{D_m}}\right) \tag{E5.4}$$

where z' is the dimensionless membrane thickness, and z_m is the membrane thickness. C_1 and C_2 are the constants that could be determined by the following boundary conditions:

$$z' = 0, z' = 1, C_A = C_{A0} \tag{E5.5}$$

$$z' = 0.5, \frac{dC_A}{dz} = 0 \tag{E5.6}$$

The solutions are

$$C_1 = 1 \tag{E5.7}$$

$$C_2 = \frac{1 - \cosh\left(z_m\sqrt{\frac{(1-\varphi)a_s\rho_m k''}{D_m}}\right)}{\sinh\left(z_m\sqrt{\frac{(1-\varphi)a_s\rho_m k''}{D_m}}\right)} \tag{E5.8}$$

Here, Thiele modulus was introduced to E5.4. The equation becomes following expression:

$$\frac{C_A}{C_{A0}} = C_1 \cosh(z'\Phi) + C_2 \sinh(z'\Phi) \tag{E5.9}$$

For a first order reaction, Thiele modulus Φ for membrane is described as:

$$\Phi = z_m\sqrt{\frac{k_m}{D_m}} = z_m\sqrt{\frac{(1-\varphi)a_s\rho_m k''}{D_m}} \tag{E5.10}$$

One would expect the plot which describes the TCE concentration change with different Thiele modules and other parameters. Also, diffusion limiting or reaction limiting conditions could be determined by different Thiele modules applied to the membrane system.

5.1.2 TCE dechlorination mechanism with adsorption and desorption on the membrane with NPs

It is known that during TCE degradation, reaction can only take place when TCE is adsorbed to Fe/Pd functionalized membrane (a control experiment was conducted by using only PVDF membrane for 24 hr without NPs' participation, nearly no TCE lost ($3.5\pm0.3\%$ lost due to volatilization) and no Cl$^-$ formation was observed). The steps of TCE dechlorination with adsorption behaviors include:

i.   TCE diffusion from the bulk solution to the Fe/Pd functionalized membrane

ii. TCE adsorption on Fe/Pd NPs surface

iii. TCE reaction on Fe/Pd NPs surface

iv. Products desorption on Fe/Pd NPs surface

v.   Product diffusion from the Fe/Pd functionalized membrane to the bulk solution.

The surface TCE degradation reaction could be described by the following equations:

Adsorption:

$$C_2HCl_3 + S \xrightarrow{\;k_{ad}\;} C_2HCl_3 \cdot S \xrightarrow{\;k_{-ad}\;} C_2HCl_3 + S \tag{E5.11}$$

Reaction:

$$\frac{5}{2}Fe + H_2O \xrightarrow{\;Pd\;} \frac{5}{2}Fe^{2+} + 5OH^- + 5H^+ \tag{E5.12}$$

$$C_2HCl_3 \cdot S + 5H^+ \rightarrow 3Cl^- + C_2H_6 \cdot S \tag{E5.13}$$

Desorption:

$$C_2H_6 \cdot S \xrightarrow{k_{de}} C_2H_6 + S \xrightarrow{k_{-de}} C_2H_6 \cdot S$$

(E5.14)
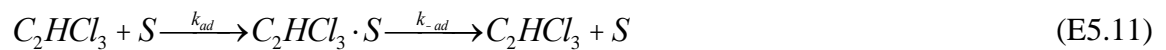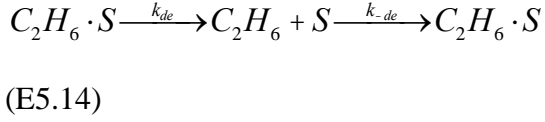
From the hypothesized surface adsorption-desorption of TCE degradation, the overall reactions could be summarized as following equations:

$$C_2HCl_3 + 2Fe + 4H_2O \xrightarrow{k_{int}} C_2H_6 + 2Fe^{2+} + OH^- + 3Cl^- \tag{E5.15}$$
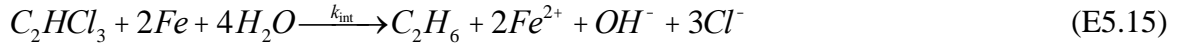
In the expression, S represents the available adsorption sites on the surfaces of NPs in membrane or in solution phase.

The overall mathematical expression of the mass balance is derived as flowing expression:

$$m_{Fe/Pd}\frac{dq_{TCE}}{dt} = -k_{int}m_{Fe/Pd}q_{TCE} - V\frac{dC_{TCE}}{dt} \tag{E5.16}$$

In the expression, V is the volume of feed solution (L), and k_{int} is the intrinsic reaction rate (h^{-1}), $m_{Fe/Pd}$ is the bimetallic loading (mg), q_{TCE} is the TCE concentration in membrane domain (mmole g^{-1}). From the adsorption aspect, another expression for TCE degradation is:

$$V\frac{dC_{TCE}}{dt} = d\left(-k_{ad}C_{TCE}V + k_{ad}m_{Fe/Pd}q_{TCE}\right) \tag{E5.17}$$

First order reaction was applied to the system and it is discovered that only part of the membrane is participating in reducing TCE in later discussion. Therefore, in this expression, a parameter δ is introduced to modify the equation and it indicates the percentage of active sites on NPs surface.

After rearranging the equation (E5.17), the following equation is obtained:

$$m_{Fe/Pd}\frac{dq_{TCE}}{dt} = -m_{Fe/Pd}K_A q_{TCE} + V\delta K_B C_{TCE} \tag{E5.18}$$

where,

$$K_A = k_{int} + k_{-ad}\delta \tag{E5.19}$$

$$K_B = k_{ad} \tag{E5.20}$$

This is the general mathematical expression which describes the model considering TCE's adsorption-desorption behaviors on the surface of Fe/Pd functionalized PAA/PVDF membrane. Several assumptions are accepted in this expression:

- TCE dechlorination reaction is irreversible;

- All reactions are at isothermal conditions;

- TCE dechlorination takes place first before releasing products into bulk solution;

- All Fe/Pd sites have homogeneous distribution and equal chance to react with adsorbed TCE.

Chaper 6   Result and Discussion

6.1 Introduction

This chapter includes the results and discussion for TCE dichlorination by Fe/Pd functionalized PAA/PVDF membrane at different conditions. Results of modeling TCE concentration change in membranes pores and TCE dechlorination mechanism with adsorption and desorption were also presented. At first, PAA polymerization in PVDF membrane was achieved and PAA pH-responsive property was investigated in water flux experiment. The Fe/Pd functionalized membranes were investigated by SEM. This provided value of NPs' size that could contribute in calculation for k_{SA} values. TCE dechlorination of using functionalized membrane was then performed at different Pd loadings and different pH comparing with solution phase by using CMC-stabilized Fe/Pd NPs, to better understand and quantify dechlorination mechanism. Finally, the results of one-dimensional model with Thiele modules and other parameters were presented to discuss TCE concentration in membrane pores and the usage of NPs in membrane system. TCE dechlorination mechanism with adsorption-desorption behavior was also discussed.

6.2 PAA/PVDF Functionalized Membrane

In this study, PAA was polymerized on the surface and in the pores of PVDF membrane. PAA, as a pH-responsive polyelectrolyte, was widely used in research area such as hydrogel synthesis (Jin and Hsieh, 2005)(He et al., 2012), control release in drug delivery (Järvinen et al., 1998)(Huh et al., 2012) and many others. PAA's pH-responsive property was investigated and the result of flux variation with different pH values was described in Figure 6.1. The result indicated that the permeability of D.I.U.F. water increased with the decreasing pH value. This result is consistent with previous reports

(Lewis et al., 2009b)(Smuleac et al., 2010). The pK_a of acrylic acid in solution is around 4.25, carbocyclic group on the PAA chain maintained non-ionized at low pH. In the pH value higher than 4.25, carbocyclic group was ionized to –COO$^-$ and H$^+$. As a result, PAA chain became more hydrophilic and expanded. With the expanded PAA chain, water flux was lower than that in lower pH. Also, linear relationship was observed to under 35 bar with 13.5% cross linker.

Also, the fraction of pore volume occupied by PAA is estimated by the weight gain of PAA-functionalized PVDF membrane in comparison to the bare PVDF membrane. The amount of PAA presented in membrane surface and pores was estimated to be 5.7 ± 0.5 mmole PAA/g dry membrane (7.4 mmole cm^{-3} membrane pore volume). Combining with the membrane thickness, the porosity, and the external surface area, the PAA gel occupied approximately 43% of the membrane pore volume, and 57% was void.
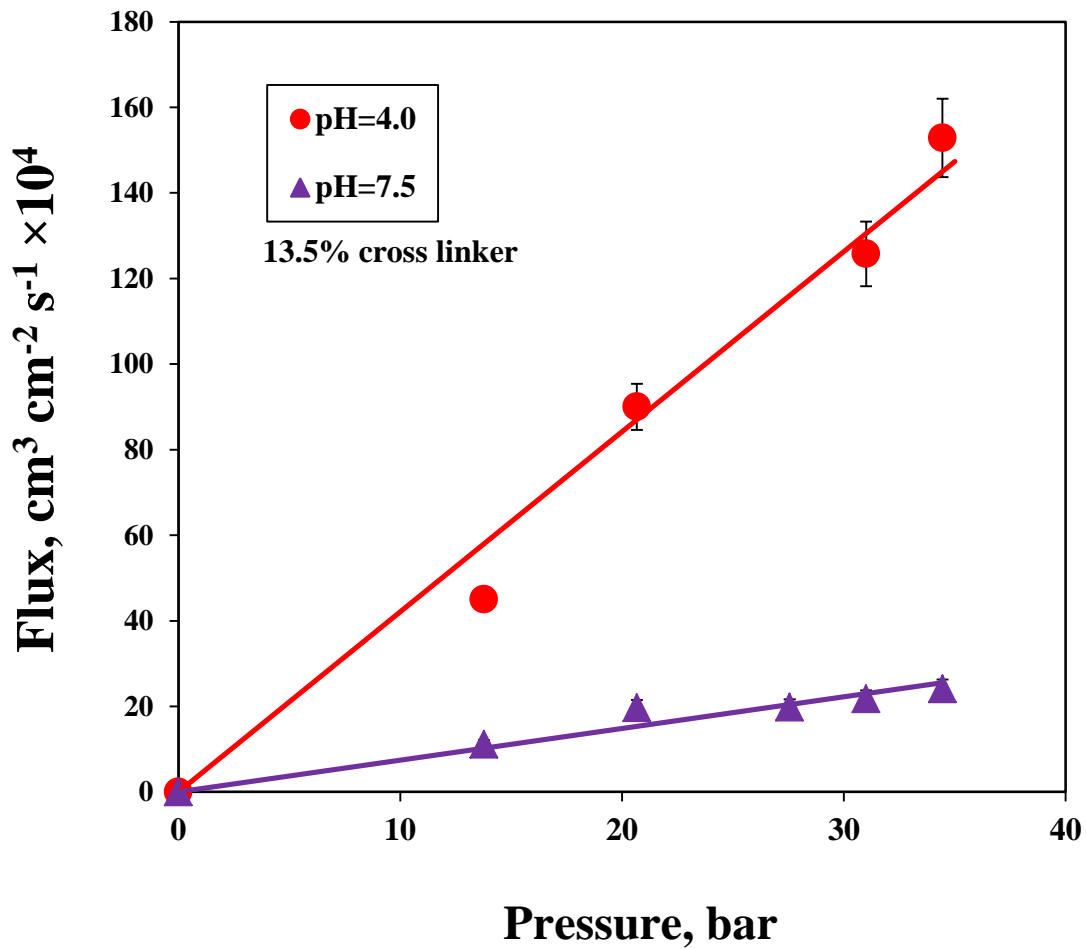
Figure 6.1 pH effect on pure water flux for PAA/PVDF membrane. (13.2 cm^2 external area)

6.3 Metal Nanoparticle Characterization

Unmodified PVDF membranes and Fe/Pd functionalized PAA/PVDF membranes were observed by SEM. Both surface and cross-section of every sample were observed at 1K, 10K and 20K magnification (see Figure 6.2, Figure 6.3, and Figure 6.4). At 10K magnification, pore structure of PVDF membrane was shown and it had large open structure that would achieve PAA polymerization. As expected, it was shown in the images that PAA successfully polymerized on the surface and inside PVDF membranes. On the surface, NPs tended to aggregate and distribute dispersedly, forming NPs of the size ranging from 50 nm to 200 nm at 20K magnification (see Figure 6.3). More uniform distribution and NP size Fe/Pd NPs were observed inside functionalized membranes. To analyze NPs size, rectangular area in Figure 6.4 was selected and 53 nanoparticles (ranging from 10 nm to 100 nm) were observed. NP size was ~50 nm at 20K magnification (see Figure 6.5).

In batch reaction using CMC-stabilized Fe/Pd NPs and sole Fe/Pd NPs, both metal NPs sizes of before and after reactions were measured by dynamic light scattering (DLS). The results indicated that the size of CMC-stabilized Fe/Pd NPs which was ~23 nm differs from that of sole Fe/Pd NPs size, ~40 nm. Stabilizer CMC was proved to enhance the uniform distribution and prevent the NPs from aggregation. Similar results were reported in previous work (He et al., 2007). In addition, it is noted by DLS that the NP size after TCE degradation experiment increased 5 to 6 times the size of fresh prepared NPs. A possible explanation to this observation is that the NPs in solution phase were oxidized after reaction, which could also be determined by the brown color of reacted solution by eyes.
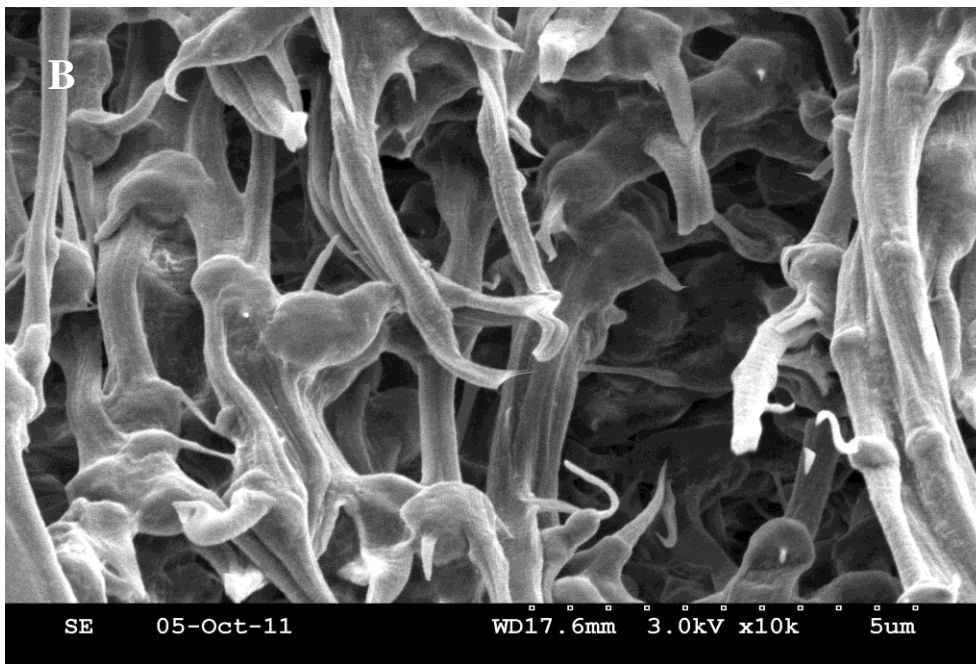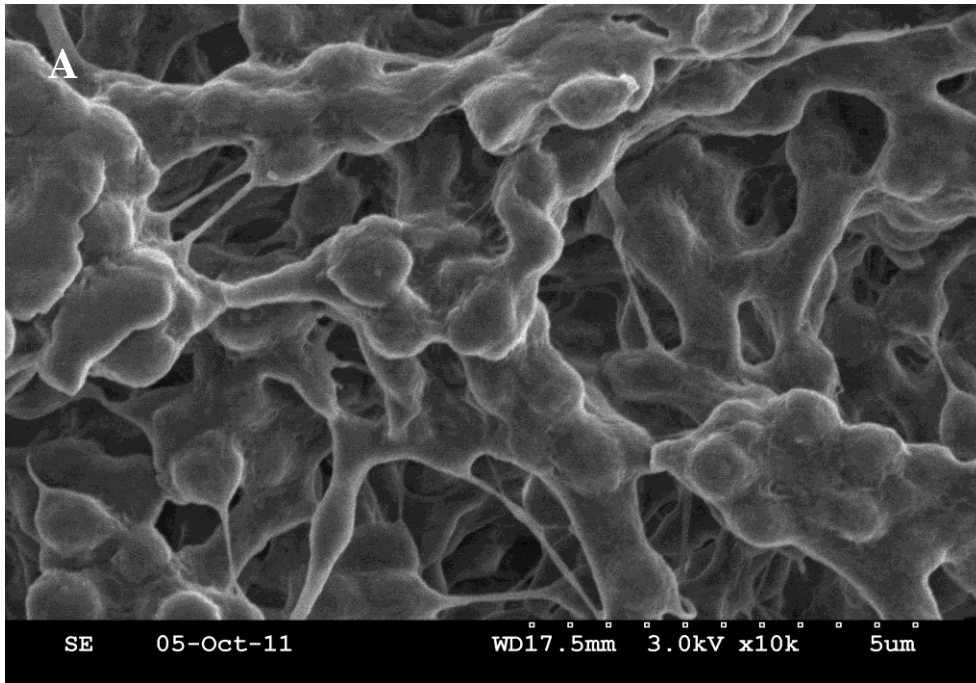
Figure 6.2 SEM characterization of PVDF membrane at 10K magnitude: (A) image of surface; (B) image of cross section. (PVDF membrane thickness: 125 μm, original poresize: 650 nm)
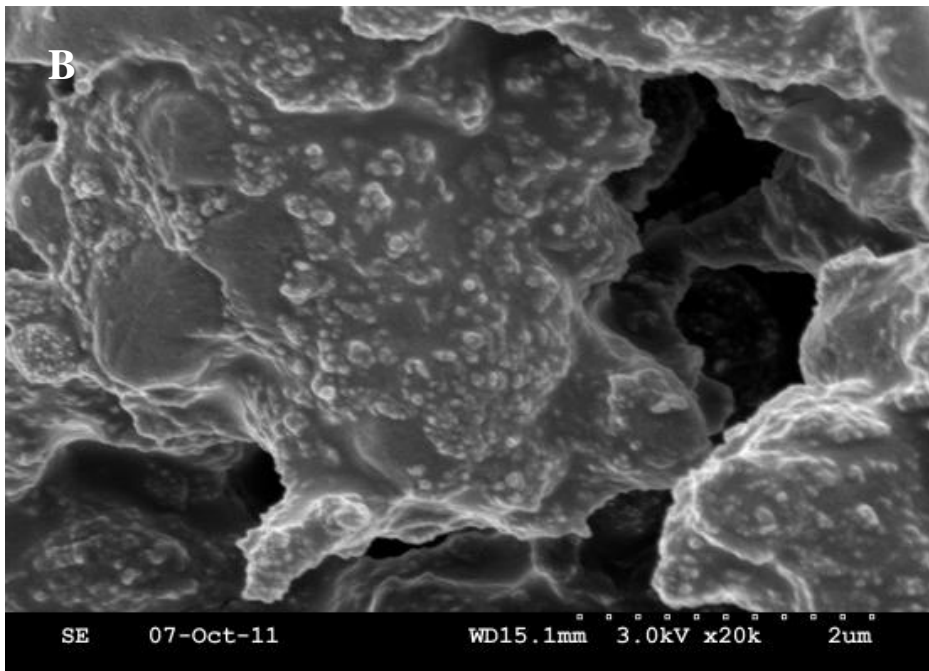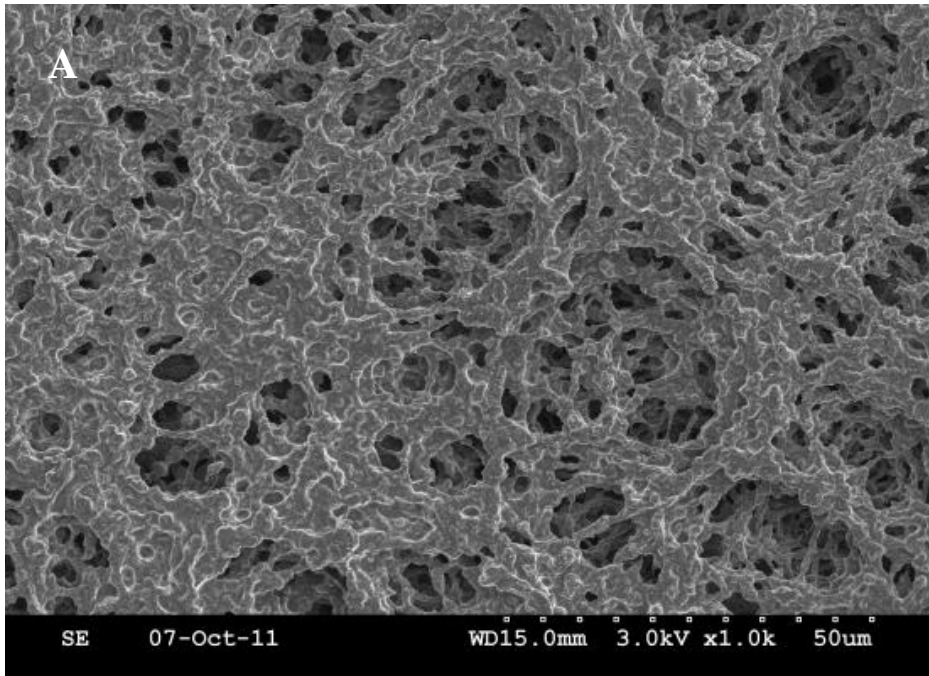
Figure 6.3 SEM characterization of Fe/Pd functionalized PAA/PVDF membrane at 1K and 20K magnitude: (A) image of surface at 1K magnitude; (B) image of surface at 20K magnitude. (PVDF membrane thickness: 125 μm, original poresize: 650 nm)
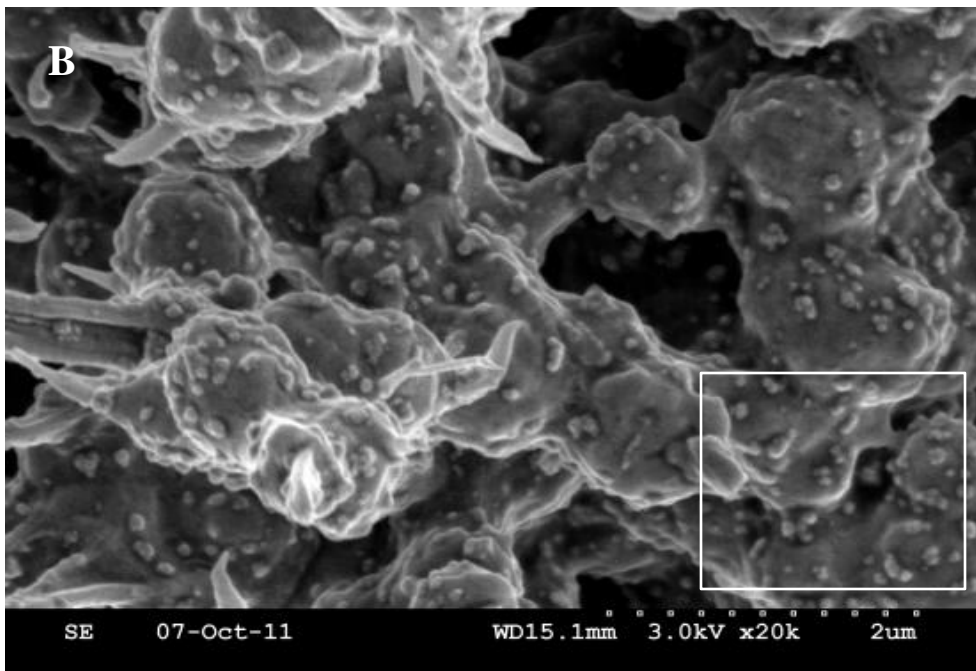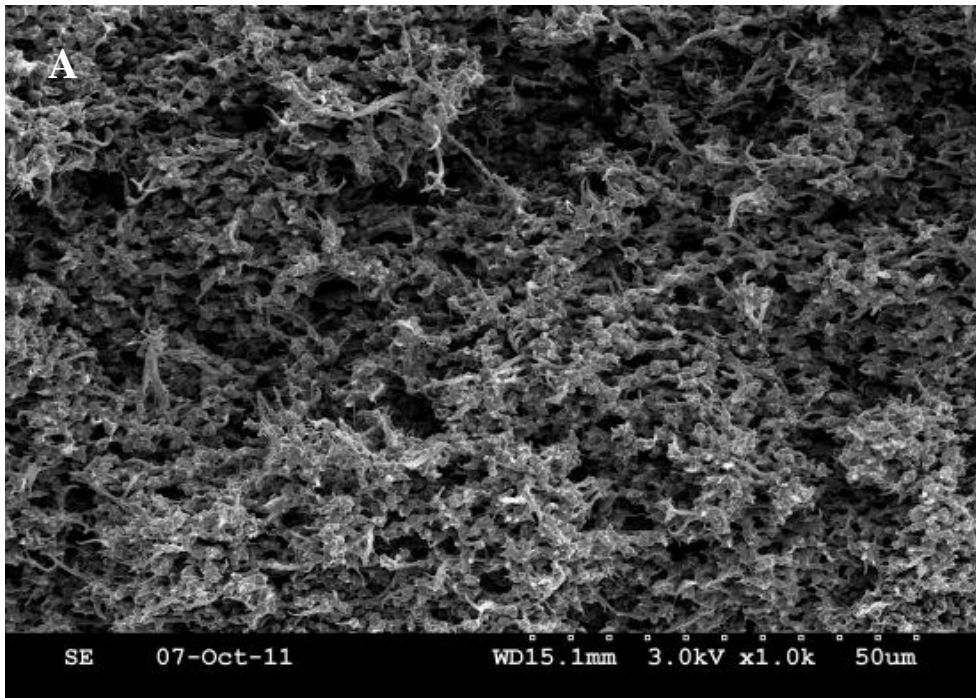
Figure 6.4 SEM characterization of Fe/Pd functionalized PAA/PVDF membrane at 1K and 20K magnitude: (A) image of cross-section at 1K magnitude; (B) image of cross-section at 20K magnitude. Rectangular area was selected to analyze NPs size. (PVDF membrane thickness: 125 μm, original poresize: 650 nm).
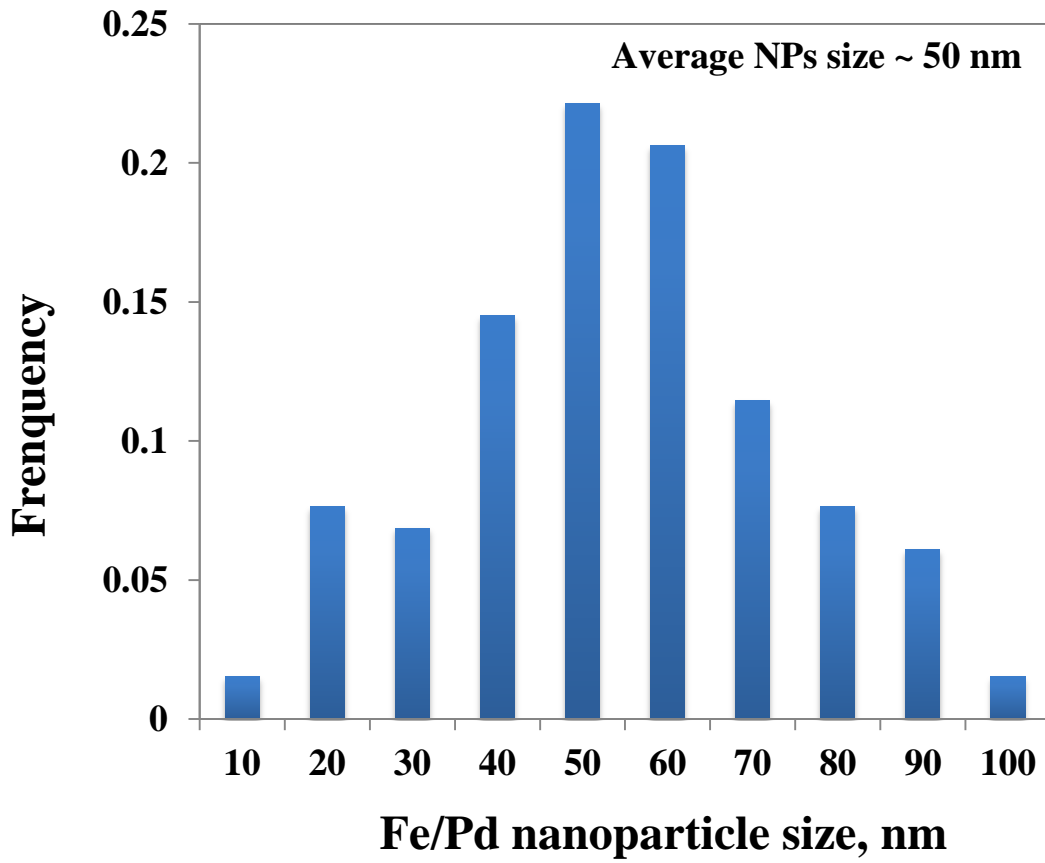
Figure 6.5 Fe/Pd NPs size frequency distribution in functionalized PAA/PVDF membranes. (Sizes of 53 nanoparticles in rectangular area from Figure 6.4 were observed and selected for analysis)

6.4 TCE dechlorination Studies

In this study, trichloroethylene (TCE) was used as a model compounds. Bimetallic Fe/Pd NPs in membrane system and in CMC-dispersed solutions were used to dechlorinate TCE. Pd NPs served as a catalyst, Fe NPs were oxidized while generating H_2 gas in reaction of TCE dechlorination.

6.4.1 Fe/Pd Nanoparticles and Reaction Rate Evaluation

Pd served as a catalyst in the reaction. The fact that bimetallic Fe/Pd system could efficiently shorten the total amount of time to dechlorinate TCE has been studied and reported by previous reports (Zhang et al., 1998)(He and Zhao, 2008). Figure 6.6 showed the results of TCE dechlorinate in solution with Fe/Pd NPs at different conditions at pH 6.4. The feed for all experiments was 40ml 30 mg L^{-1} (0.23 mmole L^{-1}) TCE solution. In all cases, Fe loading was 0.25 g L^{-1}, Pd loading was prepared as 5 wt%. Pseudo fist-order reaction kinetics was applied in TCE dechlorination, which could be described by the following equations:

$$\frac{dC_{TCE}}{dt} = -k_{obs}C_{TCE} = -k_{SA}a_s r_m C_{TCE} \qquad (E6.1)$$

where k_{SA} is the surface-area-based rate constant (L m^{-2} h^{-1}), a_s is the surface area of the NPs (m^2 g^{-1}), and ρ_m is the mass concentration of the NPs in solution (g L^{-1}). The results indicated that the system of CMC-stabilized Fe/Pd achieved the highest k_{SA} value among all, which was 1.061 L m^{-2} h^{-1}. Without the presence of catalyst Pd NPs, one would expect that the sole Fe NPs system was the least favorable to TCE dechlorination. The results agreed with the expectation that the sole Fe NPs system obtained the lowest k_{SA}
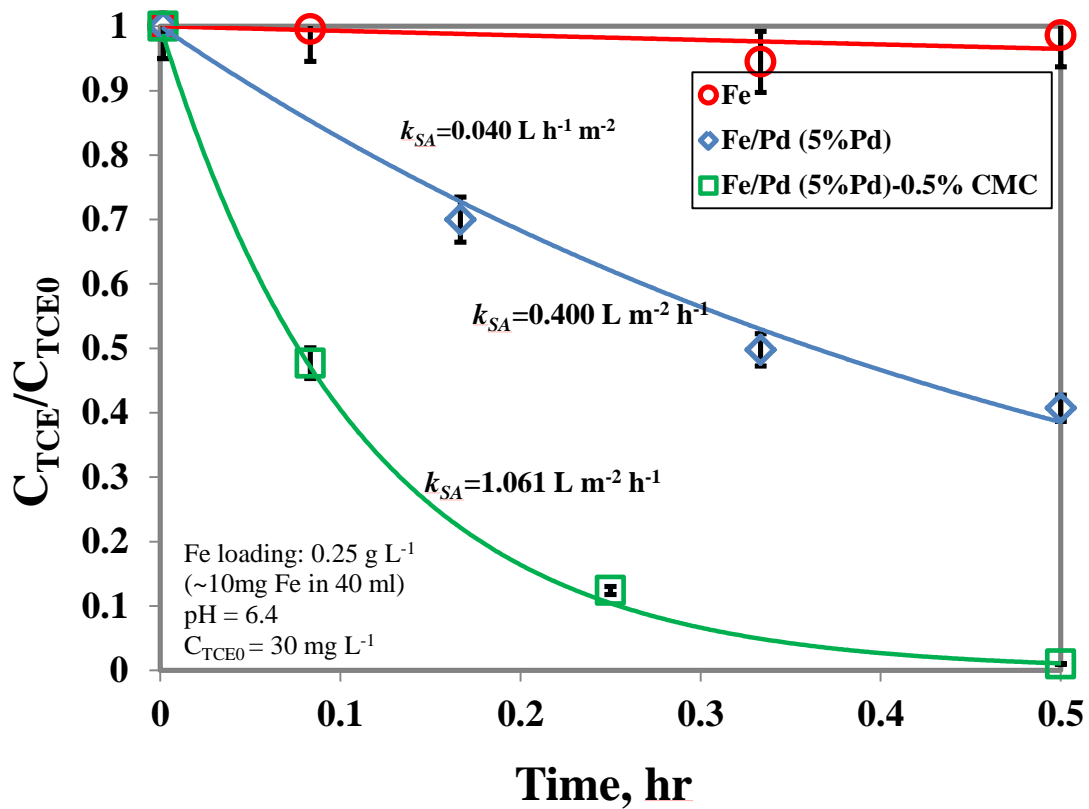
Figure 6.6 TCE dechlorination using Fe/Pd NPs and CMC-stabilized Fe/Pd NPs with 0.25 g L^{-1} Fe loading and 5 wt% Pd loading at pH 6.4 in batch reaction. (Feed solution: 40 ml 30 mg L^{-1} TCE)

value among all, which was 0.040 L m^{-2} h^{-1}, about 1/25 of the highest value. Similar results were consistent with the experiment data from previous reports (Wang and Zhang, 1997)(He and Zhao, 2008).

For CMC and membrane, they both served as stabilizers to enhance the homogeneous distribution of NPs, also to prevent the metal NPs forming aggregation in the solution. In order to compare the effectiveness of both systems, a TCE dechlorination experiment was operated in Fe/Pd modified PAA/PVDF membrane system with the same metal loading and pH. The k_{SA} value for membrane-immobilized NPs was 0.616 L m^{-2} h^{-1} (see Figure 6.7), which was lower than the value of CMC-stabilized Fe/Pd NPs. It was investigated that the NP size of CMC-stabilized obtained from SEM and DLS (~23nm) were smaller than that of membrane-mobilized NPs (~50nm). It was also observed in Figure 6.3 and Figure 6.4 that the NPs imbedded in PAA layer did not completely contribute to TCE dechlorination. Also, there's mass transfer resistance in membrane system where TCE has to diffuse through membrane surface into membrane pores to contact with NPs in order to be reacted. Therefore, with more active surface area and active sites, TCE had better contact with NPs to be destroyed and transformed into products in CMC-stabilized system. The result was reasonable and expected.

Even though CMC-stabilized NPs achieved a higher reaction rate than that in membrane system, the suspension of Fe/Pd NPs in the solution could cause problems in practical application, such as metal recapture and metal loss. As what's mentioned earlier, size of CMC-stabilized Fe/Pd increased 5-6 times after reaction and it was difficult to rejuvenate the activity because of the NPs' aggregation. Therefore, membrane served as a better immobilization platform for Fe/Pd NPs to suppress the NPs loss during the reaction.
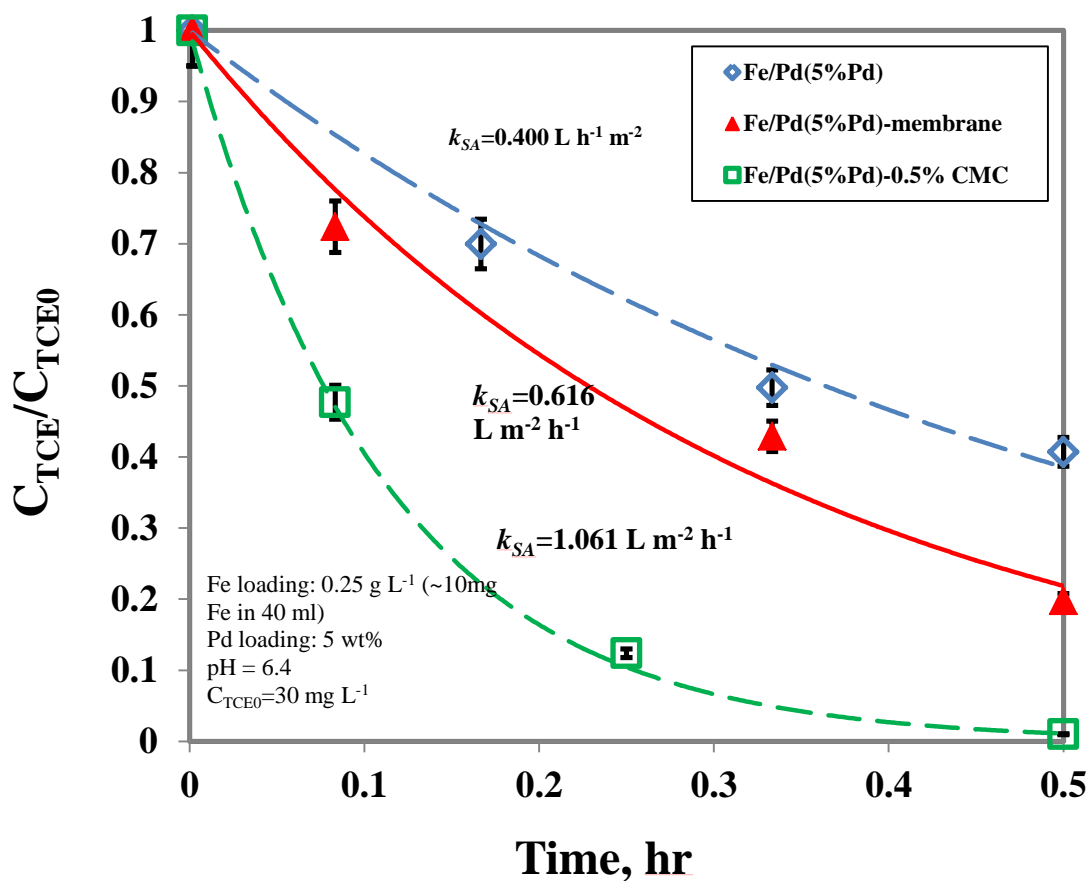
Figure 6.7 TCE dechlorination using Fe/Pd immobilized PAA/PVDF membrane with 0.25 g L^{-1} Fe loading and 5 wt% Pd loading at pH 6.4. (Comparison with non-membrane systems) For membrane: 13.2 cm^2 external area, Fe/Pd nanoparticle size d_p: 50 nm. All experiments were in batch reaction.

6.4.2 pH Effect on TCE Dechlorination

pH value is one important aspect to effect TCE dechlorination (Liu and Lowry, 2006)(Chen et al., 2001). In strong acid environment, the presence of H^+ is favorable to the reaction to proceed forward according to reaction equation (21). On the contrary, reaction is retarded by the presence of high OH^- concentration. Although lowering pH could increase k_{SA} values, it also accelerates Fe NPs' corrosion to decay its activity for TCE degradation (Chen et al., 2001). In this study, pH range for TCE dechlorination experiments was between 4 and 10.

In the reductive mechanism of TCE dechlorination, TCE and H^+ both can oxidize Fe^0 to Fe^{2+} by forming $C_2H_nCl_{4-n}$ (n=2,3,4) and Fe^{2+} (TCE dechlorination and Fe corrosion). The competition between TCE and H^+ to react with Fe^{2+} reveals that H_2 evolution has an impact on TCE dechlorination (Liu and Lowry, 2006). H_2 evolution and TCE dechlorination could be described by following expressions using ZVI treatment:

$$\frac{dH_2}{dt} = k_{H_2} a_s [Fe^0][H^+] \tag{E6.2}$$

$$\frac{dC_{TCE}}{dt} = -k_{TCE} C_{TCE} a_s [H^+]^{0.16} \tag{E6.3}$$

where a_s is the surface area area (m^2 g^{-1}).

It can be concluded that it's favorable to TCE dechlorination at high TCE concentration and low pH with certain amount of Fe loading. However, TCE dechlorination rate not only depends on H^+ and Fe^0 amount, other chemical or physical factors could also control reaction rate, such as by catalytic reaction and particle sizes.

TCE dechlorination experiments were conducted in 40 ml 30 mg L^{-1} TCE solution at different pH values with 0.25 g L^{-1} Fe loading, 5 wt% Pd loading by using PAA/PVDF membrane. With previous elaboration, one would expect to notice the k_{SA} value increases with decreasing pH value in certain range. The experimental data correlated well with expectation that it was observed that k_{SA} of TCE dechlorination in modified PAA/PVDF membrane increased with lowering the pH value (see Figure 6.8). TCE was completely degraded after 2.5 hours at pH 6.4, and k_{SA} value was 0.616 L m^{-2} h^{-1} which was almost 1 order of magnitude the value at pH 9.6, 0.120 L m^{-2} h^{-1}.

Cl$^-$, as one of the main product, its concentration was investigated as well. As described in section 4.3.8, Cl$^-$ concentration was measured by applying calibration curve. The ratio of mmoles of Cl$^-$ over mmoles of TCE consumed was measured with time. The result in Figure 6.9 showed an excellent agreement with the change of TCE concentration measured by GC-MS (see Figure 6.8). The result also indicated that most of TCE was completely dechlorinated into ethene (or ethane) and Cl$^-$ without forming toxic intermediates such as dichloroethene, vinyl chloride by Fe/Pd bimetallic treatment. Our observation was in an agreement with previous reports (He et al., 2007).

TCE dechlorination experiments were also investigated at different pH by using CMC-stabilized Fe/Pd NPs. The result was shown in Figure 6.10 and Figure 6.11. In Figure 6.10, we found that k_{SA} had similar tendency with changing pH comparing to that in membrane system. Chloride concentration was also measured as the ration of mmoles of Cl$^-$ over mmoles of TCE consumed at different time interval (see Figure 6.11). It also agreed well with the TCE degradation result from GC-MS. In both CMC-stabilized Fe/Pd and Fe/Pd modified membrane treatments, it was found that the k_{SA} was negatively

correlative with pH value (see Figure 6.12). Although PAA has pH-responsive property and there is mass transfer resistance in membrane system, the result indicated that both systems had similar k_{SA} tendency with pH at certain range and the performance of modified PAA/PVDF membrane is stable and consistent.

The relation between k_{SA} and pH was investigated in both systems as well. The k_{SA} value of CMC-stabilized Fe/Pd NPs was around twice that value in membrane system at the same pH range (see Figure 6.12). It is noted that k_{SA} was approximately proportional to pH with the presence of CMC-stabilized Fe/Pd NPs (R^2=0.9926). This linear relation was similar with previous report by using only ZVI in TCE dechlorination between pH 3.8 and 8.0 (Chen et al., 2001). For membrane system, linear relation was not obvious between k_{SA} and pH, this could relate to the mass transfer resistance when TCE reacted with Fe/Pd NPs. Also, the impact of PAA pH-responsive property on TCE dechlorination was not fully studied and understood. It could play a role in the non-linear relation between k_{SA} and pH in membrane system as well. More quantitative information is needed in this case.

Data from Figure 6.8 and Figure 6.9 analyzed TCE dechlorination and Cl⁻ formation by Fe/Pd functionalized membrane at different pH. Data were obtained by collecting sample every 10 to 30 min, and then analyzed by GC/MS for TCE and chloride electrode for Cl⁻ concentration. Same procedure operated by using CMC-stabilized Fe/Pd NPs, results showed in Figure 6.10 and Figure 6.11. Second metal's participation could dramatically increase reduction rate. In addition, it is reported earlier that nearly no intermediates formation was observed after TCE dechlorination by using Fe/Pd NPs (He and Zhao, 2005), and final products of TCE dechlorination are mainly Cl⁻ and ethane

(ethane). One could expect that ratio of Chloride to TCE maintain at 3:1 through the dechlorination (with sufficient Fe/Pd NPs). Figure 6.13 showed the plot of mmoles of Cl^- produced to mmoles of TCE consumed in the reaction, where dash line in the figure stands for the stoichiometric ratio (Cl^- : TCE=3:1). Every data point with same symbol represented the sample obtained at different time. It is observed that in both treatments (by CMC-stabilized and membrane-immobilized Fe/Pd NPs), chloride released while degrading TCE, and chloride formation was ±8% of stoichiometric value. This figure also indicated that the change of TCE concentration did not affect the activity of Fe/Pd in this dosage. 0.25 mg L^{-1} Fe loading corresponds to 0.178 mmoles total Fe NPs in 40 ml TCE solution, the value is excessive compared to stoichiometric value needed to dechlorinate all the TCE in solution calculated by E3.6, E3.7, E3.8 (30 mg L^{-1} TCE in 40mL solution needs 0.037 mmoles of Fe NP to complete degradation). With adequate Fe loading and Pd's participation, the result is expected as showed in the graph.

51
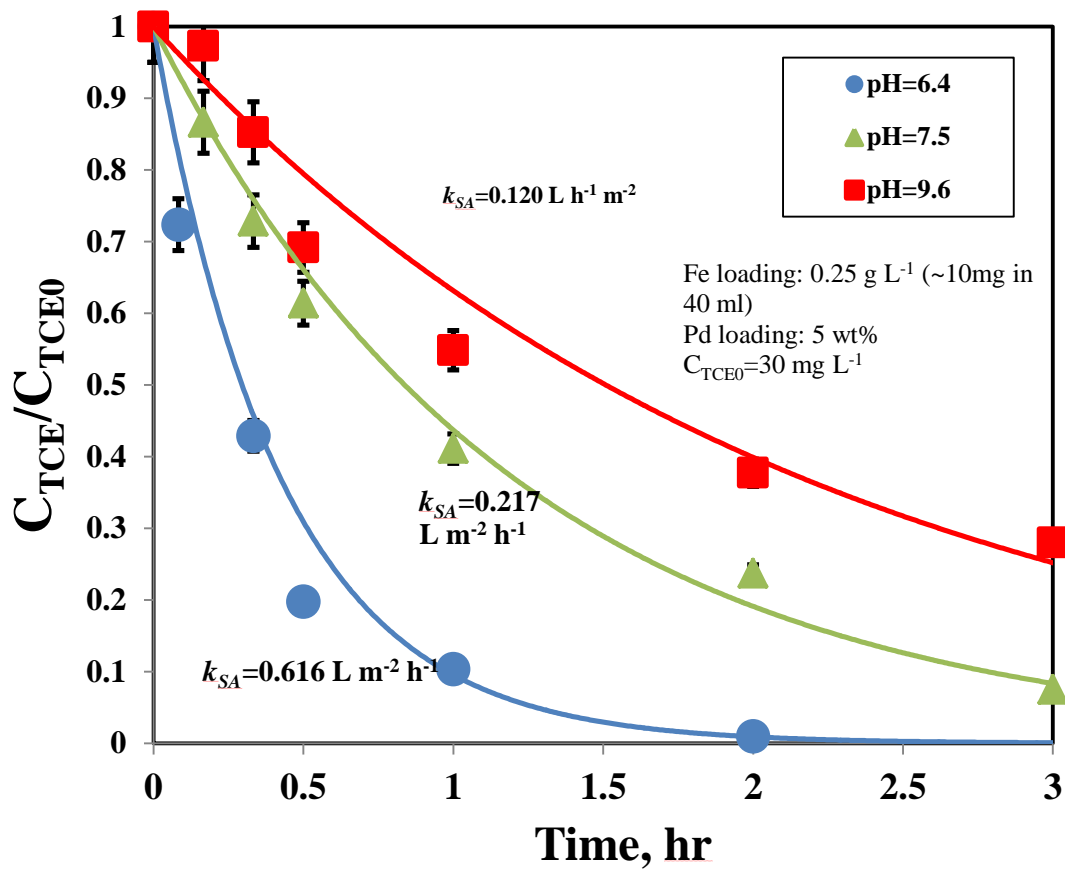
Figure 6.8 TCE dechlorination using Fe/Pd functionalized PAA/PVDF membrane at different pH with 0.25g L^{-1} Fe loading and 5 wt% Pd loading in batch reaction. (Feed solution: 40 ml 30 mg L^{-1} TCE, Fe/Pd nanoparticle size d_p: 50 nm)
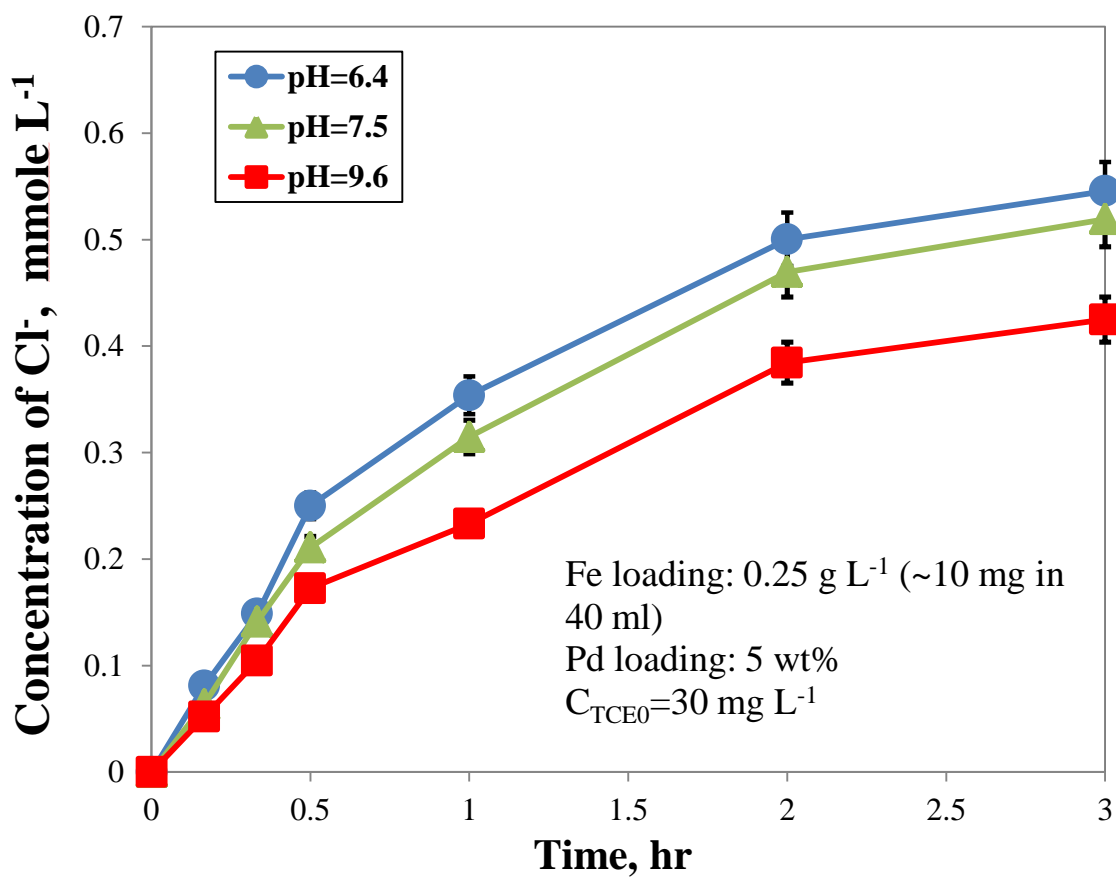
Figure 6.9 Chloride formation in TCE dechlorination using Fe/Pd functionalized PAA/PVDF membrane at different pH with 0.25 g L^{-1} Fe loading and 5 wt% Pd loading in batch reaction. (C$_{TCE0}$: 30 mg L^{-1}, Fe/Pd nanoparticle size d_p: 50 nm)
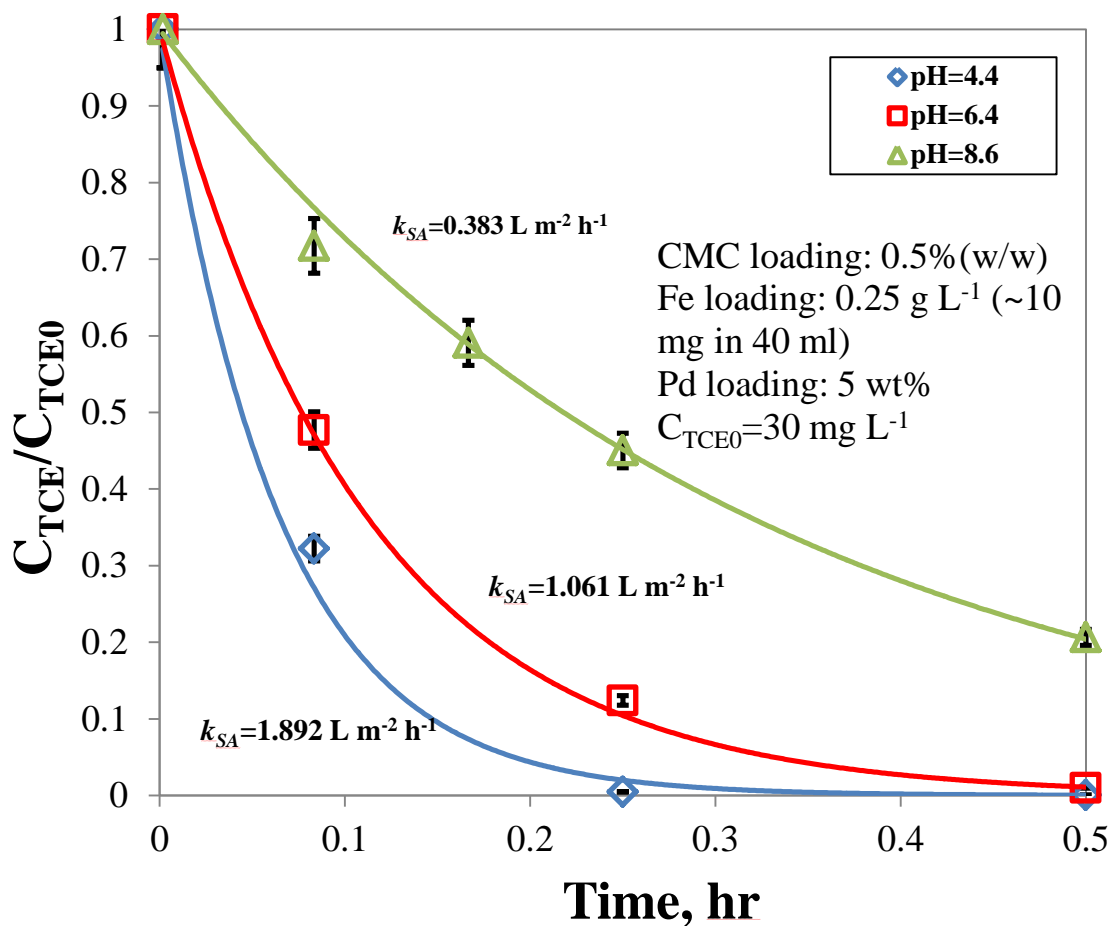
Figure 6.10 TCE dechlorination using CMC (0.5 wt%)-stabilized Fe/Pd NPs at different pH with 0.25 g L^{-1} Fe loading and 5 wt% Pd loading in batch reaction. (Feed solution: 40 ml 30 mg L^{-1} TCE, Fe/Pd nanoparticle size d_p: 23 nm)
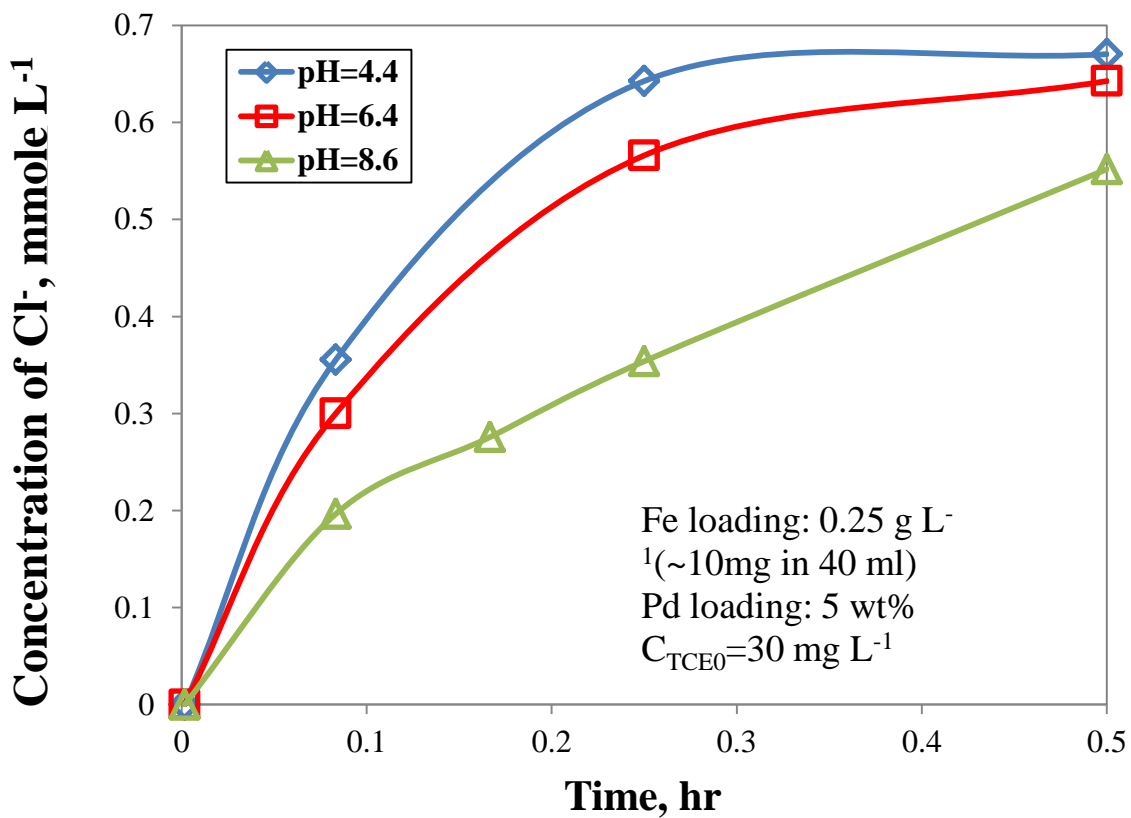
Figure 6.11 Chloride formation in TCE dechlorination using CMC (0.5 wt%)-stabilized Fe/Pd NPs at different pH with 0.25 g L^{-1} Fe loading and 5 wt% Pd loading in batch reaction. (Feed solution: 40 ml 30 mg L^{-1} TCE, Fe/Pd nanoparticle size d_p: 23 nm)
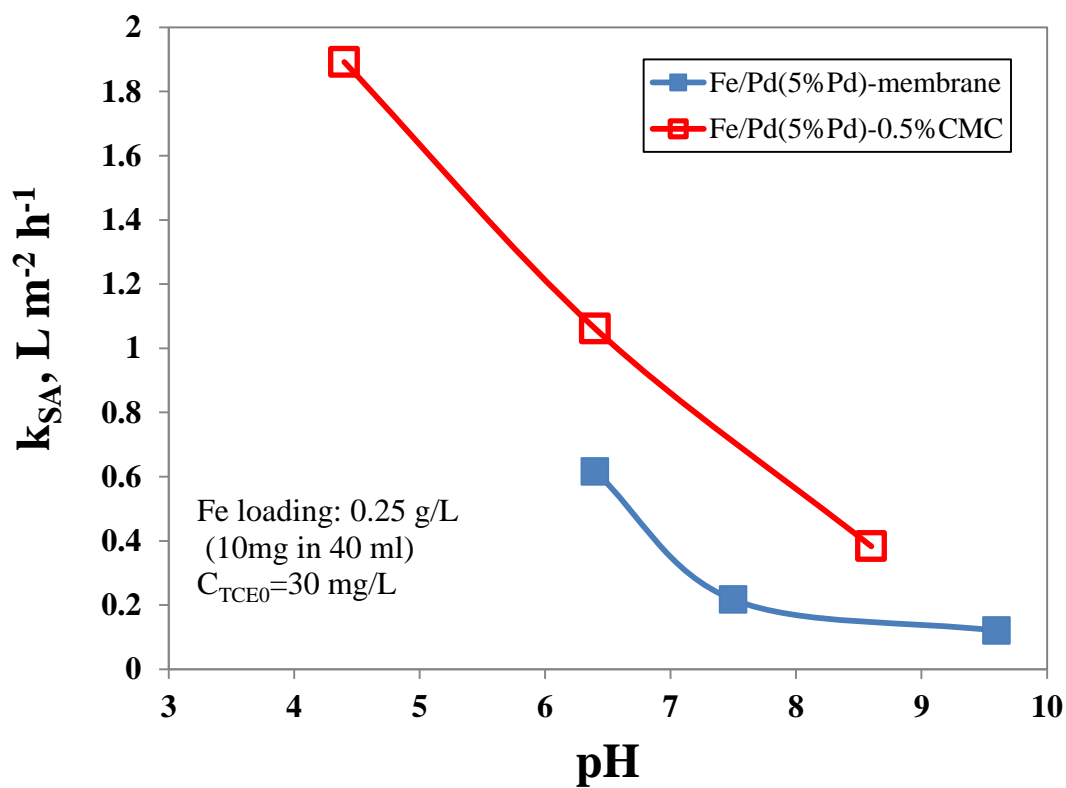
Figure 6.12 Effect of different pH on surface-area reaction rate constant by using Fe/Pd NPs at membrane and CMC in solution with 0.25 g L^{-1} Fe loading for TCE dechlorination (Feed solution: 40 ml 30 mg L^{-1} TCE). All experiments were in batch reaction.
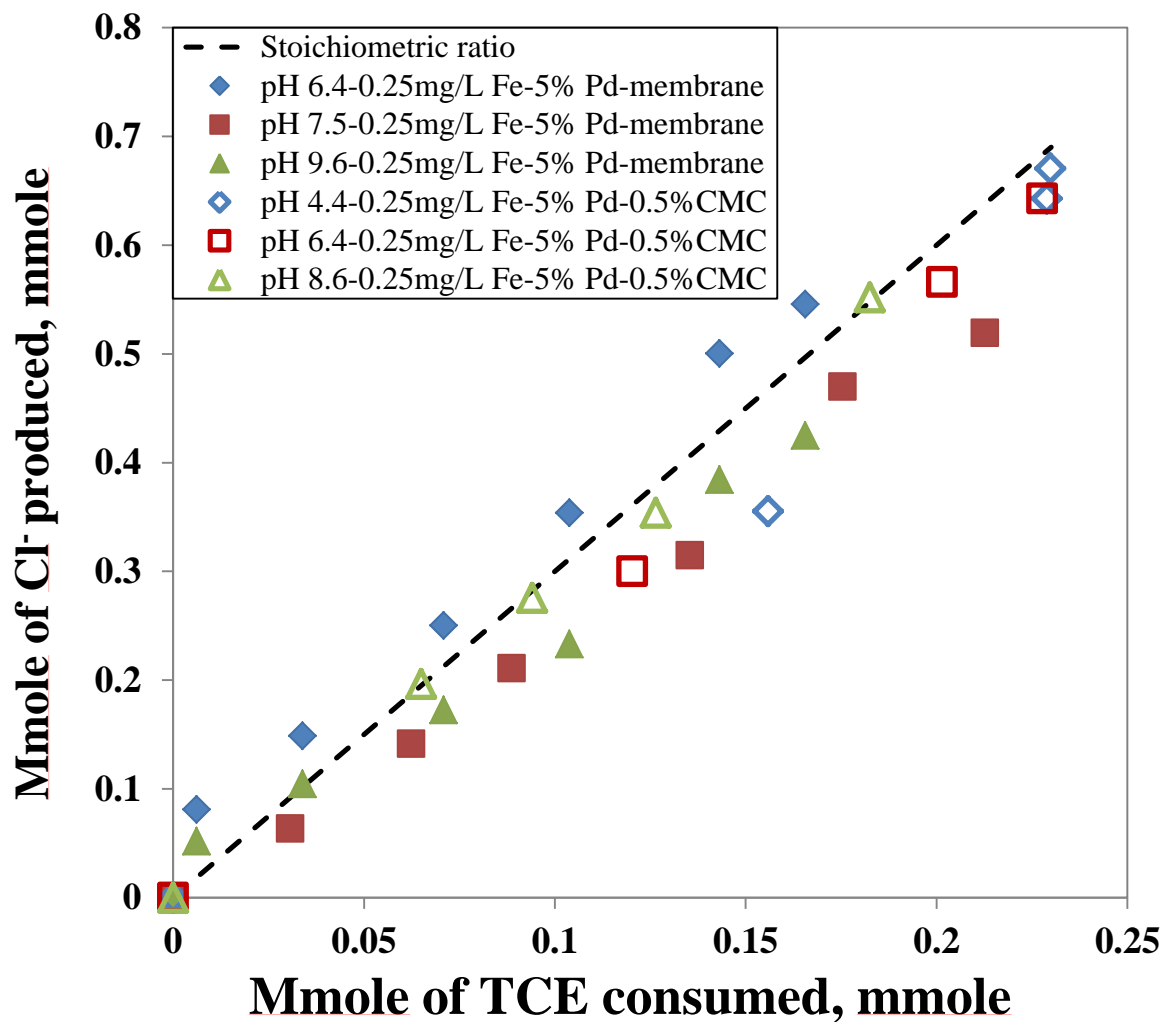
Figure 6.13 Plot of mmoles of Cl⁻ produced to mmoles of TCE consumed by membrane immobilized and CMC-stabilized Fe/Pd NPs at different pH. (Data collected at different reaction time for same system)

6.4.3 Effect of different metal loading on TCE dechlorination

Another important effect on TCE dechlorination is Pd loading. During TCE dechlorination, Fe NPs reacted with H_2O to generate H_2 as product, and Pd served as catalyst to accelerate reaction. It was observed in Figure 6.6, with only Fe NPs' participation, longer time was needed to completely destroy TCE and toxic intermediate were forming during the reaction according to previous reports (Tratnyek et al., 1997)(Zhang, 2003). With the presence of Pd, it is expected to achieve higher value of k_{SA} without forming intermediates. Modified PAA/PVDF membrane with different metal loadings was applied in TCE dechlorination experiments at pH 6 for 2 hours (see Figure 6.14). H_2O is also a reactant, TCE cannot be de degraded without the contact with water on the surface on NPs. Theoretically, it is expected that no TCE chlorinated with 100 % Pd coverage on Fe NPs since no water could react with Fe NPs. Similar result was reported in previous report by using Au/Pd bimetallic NPs to chlorinate TCE (Nutt et al., 2006). In this study, the maximum amount of Pd prepared was 5 wt% and 2.8 mol% based on Fe loading. With the same wt% of Pd, one would expect that the system with higher Fe loading obtained higher k_{SA} value. Also, with same amount of Pd but different Fe loadings, systems could end up with same k_{SA} value at the pH with same reaction time. Experiment data indicated that k_{SA} was proportional to Pd loading (R^2=0.9901) (see Figure 6.15), which was in an agreement with previous reports of TCE dechlorination (Smuleac et al., 2010) and DiCB dechlorination (Xu and Bhattacharyya, 2008). The coverage of Pd on Fe NPs surface was calculated based on 50 nm diameter of Fe NPs and 0.0787 nm^2 (Nutt et al., 2005). The calculation result indicated that there was around 51% Pd coverage.
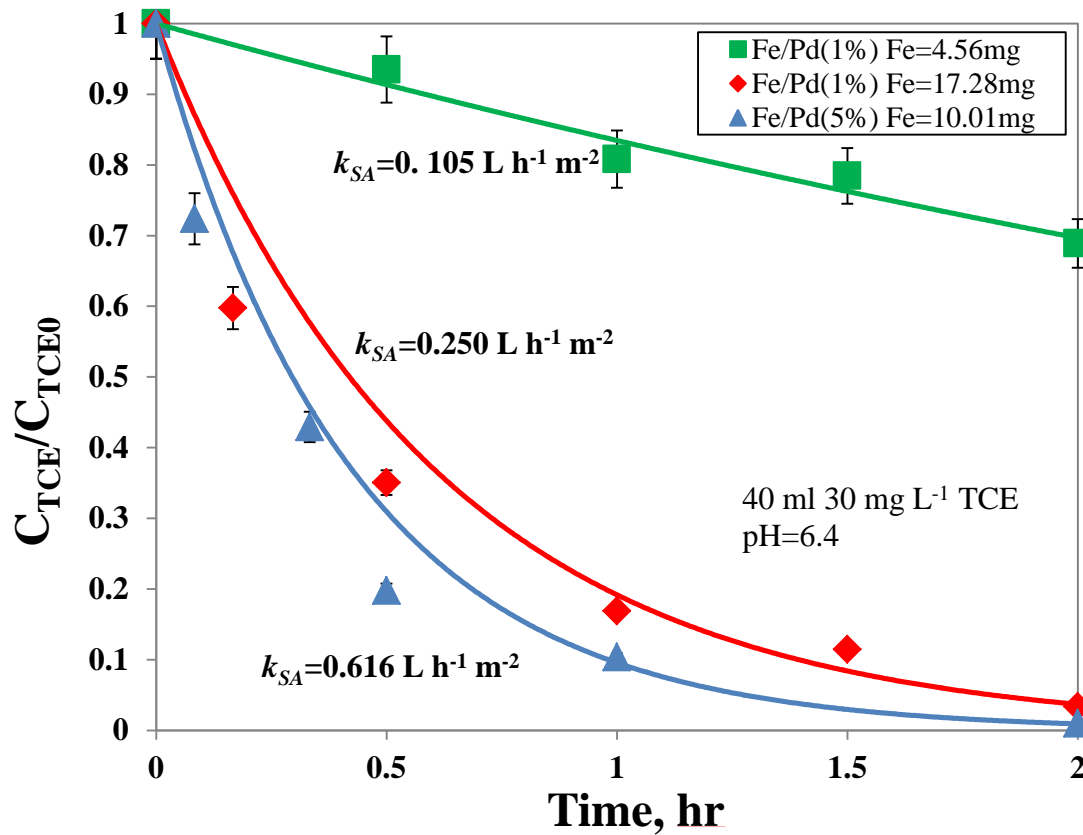
Figure 6.14 TCE dechlorination using Fe/Pd functionalized PAA/PVDF membrane with different metal loadings at pH 6.4 in batch reaction. (External area: 13.2 cm^2, Fe/Pd nanoparticle size d_p: 50 nm)
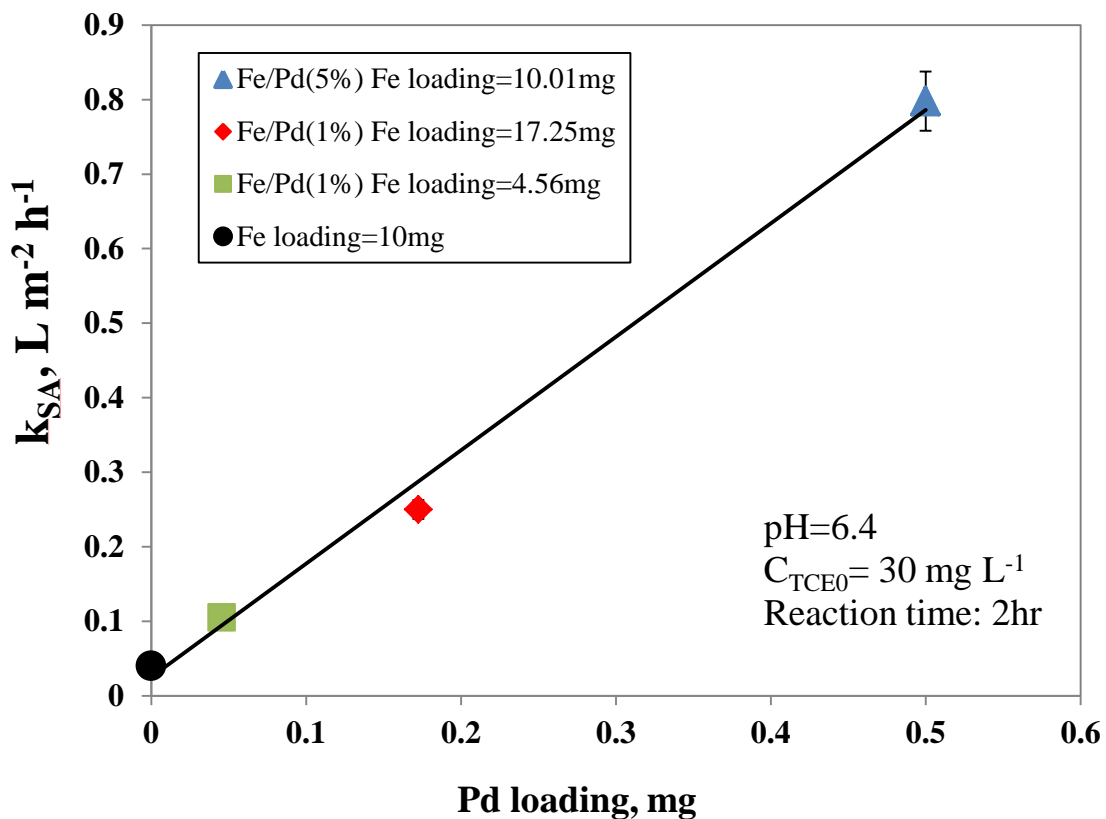
Figure 6.15 TCE dechlorination using Fe/Pd functionalized PAA/PVDF membrane with different metal loadings at pH 6.4 in batch reaction. (External area: 13.2 cm^2, Fe/Pd nanoparticle size d_p: 50 nm)

6.5 TCE Batch Dechlorination Modeling

Prior work done in this study focused on TCE dechlorination reaction, and different effects on reduction reaction. Fe/Pd successfully functionalized PAA/PVDF membrane performed highly active degradation on TCE dechlorination. Results were analyzed at different pH and different bimetallic loading. However, quantitative experiment results do not reflect the reaction occurred in membrane matrix. Functionalized membrane has mass transfer resistance compared to solution reaction (by CMC or other stabilizers). This indicates that diffusion control might be a drawback for membrane system in lowering dechlorination reaction rate (compared to CMC-stabilized NPs system, see Figure 6.12). However, quantitative data of reactions in membrane pores have never been reported by literature so far. Modeling TCE concentration profile in membrane pores and different parameters' impact give us details of the exact description of dechlorination scenario in membrane pores.

6.5.1 One-Dimensional Model and parameter discussion

Thiele modulus Φ is a parameter that describes the relation between reaction and diffusion in a specific system. Thiele modulus, in this study, could be effected by several parameters such as reaction rate, pH, NPs loading and void volume fraction. These effects perform in the model in terms of NPs surface area a_s, surface-normalized reaction rate k'', mass concentration, diffusivity D_m. TCE dechlorination profile could be observed by changing one parameter while maintaining others.

To investigate the impact of Thiele modulus on TCE dechlorination with one-dimensional model, equation E5.8 was written below for convenience

$$\frac{C_A}{C_{A0}} = C_1 cosh(z'\Phi) + C_2 sinh(z'\Phi) \tag{E5.9}$$

C_1, C_2 is calculated by E5.7 and E5.8.

By applying different value of Thiele module to E5.9, Figure 6.16 shows the results of the change of TCE concentration when it diffuses through membrane in z direction. As what's observed from Figure 6.16, with Thiele modules increasing, reaction rate dominates and it is diffusion limited. This result is correspondent with that in Figure 6.17 and Figure 6.18. With higher reaction rate (performed in value of Φ and k'') and lower value of diffusivity, all TCE is dechlorinated by NPs before it penetrates through membrane. If NP is with only iron, intermediates formation could be further dechlorinated in pores; if NPs has second metal's participation, final product Cl$^-$ is performed when TCE is completely degraded. This result is expected and it shows the relation among reaction rate, diffusion and TCE dechlorination in a directed way describing TCE dechlorination in membrane pores.

Not only reaction rate, diffusivity of TCE affect the dechlorination profile, but also other parameter described in equation E5.4. Effect of these parameters is observed by changing particular parameter while changing others. Void volume in pores is illustrated in Figure 4.1. Although PAA and NPs were synthesized in membrane pores, there is still around 57% void volume in pores. Especially in convective flow, TCE could penetrate membrane in a fast speed through a 'free' way that allows no contact with NPs. In this case, actual efficiency of NPs is higher than what's observed form bulk solution since less TCE is chlorinated. In Figure 6.19, impact of different values of void volume fraction on TCE dechlorination profile was performed. When the void volume occupies all the free volume in membrane, no TCE is dechlorinated. On the contrary, Less TCE

without reaction flows through membrane, more NPs are oxidized and more efficient to

membrane is.

Figure 6.16 Plot of equation E5.9 describing TCE concentration change within Fe/Pd functionalized PAA/PVDF membrane at different Thiele modulus.

Figure 6.17 Plot of equation E5.4 describing TCE concentration change within Fe/Pd functionalized PAA/PVDF membrane at surface-area-based rate constant k'' with constant φ, a_s, ρ_m and D_m.

Figure 6.18 Plot of equation E5.4 describing TCE concentration change within Fe/Pd functionalized PAA/PVDF membrane at diffusivity D_m with constant φ, k'', a_s and ρ_m.

Figure 6.19 Plot of equation E5.4 describing TCE concentration change within Fe/Pd functionalized PAA/PVDF membrane at different void volume fraction φ with constant k'', a_s and ρ_m and D_m.

NPs size and loading also play an important role in this model. In section 6.4.2, even though CMC-stabilized NPs had metal loss and other drawback, but CMC-stabilized NPs had smaller size than that of membrane-immobilized NPs, thus achieved higher k_{SA}. Smaller size of nanoparticles contributes to larger active surface area that provides more sites for TCE to attach and react in solution and in membrane. Also, different Pd loading in section 6.4.3 was discussed by dechlorinating TCE. It was found that reaction rate was proportional to Pd loading in this study. It is expected that more TCE are dechlorinated with more metal loading and larger surface area. The result of Figure 6.20 and Figure 6.21 showed an agreement with expectation. More TCE is dechlorinated by NPs with larger surface areas (smaller nanoparticle size) and large mass concentration (more metal loading).

From all the model results from Figure 15-20, the most effective TCE dechlorination profile all showed that TCE dechlorination completion is achieved before TCE penetrates to the center of membrane (symmetric profile). This means that only part of the membrane with Fe/Pd NPs is used, and the reaction rate represents the reduction reaction by using partial membrane. Correction is needed to amend the observed reaction rate in bulk solution, especially for those systems with higher metal loading and at lower pH range. Also, it implied that thinner membrane could have the same performance but higher reduction efficiency in TCE dechlorination.

This model discussed a TCE concentration profile in membrane pores that has never been reported in literature. Fe/NPs functionalized PAA/PVDF membrane for TCE dechlorination is a complicated system because of PAA responsive property, Fe/Pd corrosion, nanoparticle size and reaction mechanism. TCE concentration profile is

determined by different parameters, and the effect of parameters has been studied by describing trends of TCE concentration change. This model not only describes TCE concentration change in pores, but also indicates that not all NPs in membrane participate in TCE dechlorination in some conditions. Reaction efficiency of dechlorination in membrane needs modification to fit the actual TCE degradation profile.
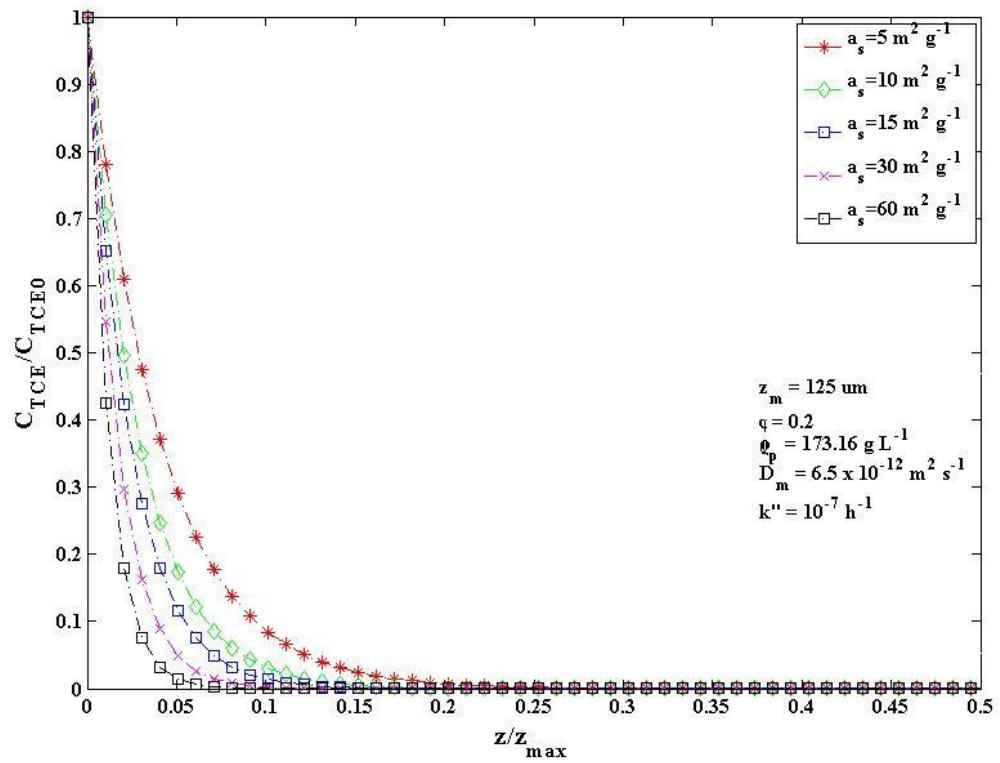
Figure 6.20 Plot of equation E5.4 describing TCE concentration change within Fe/Pd functionalized PAA/PVDF membrane at surface area a_s with constant φ, k'', ρ_m and D_m.
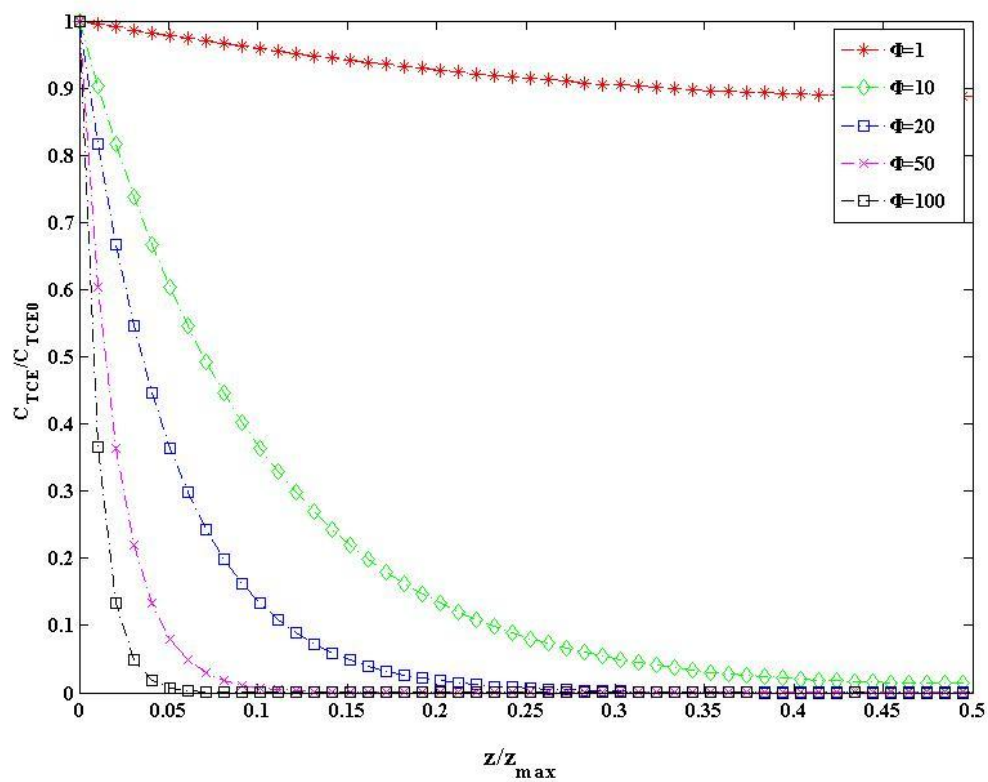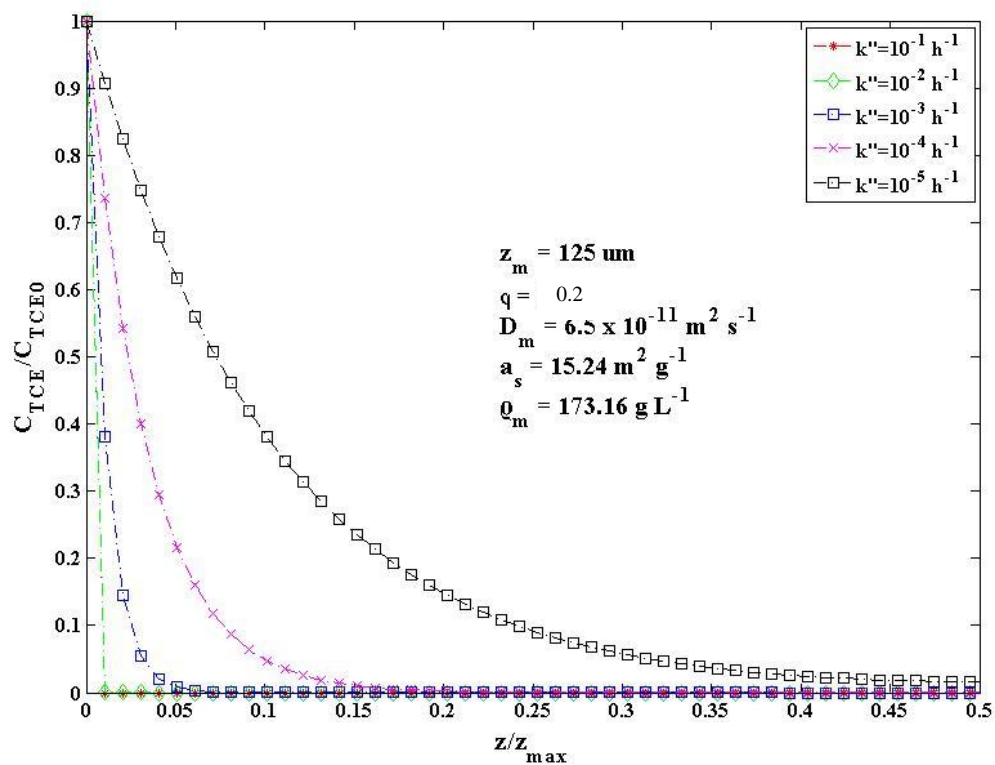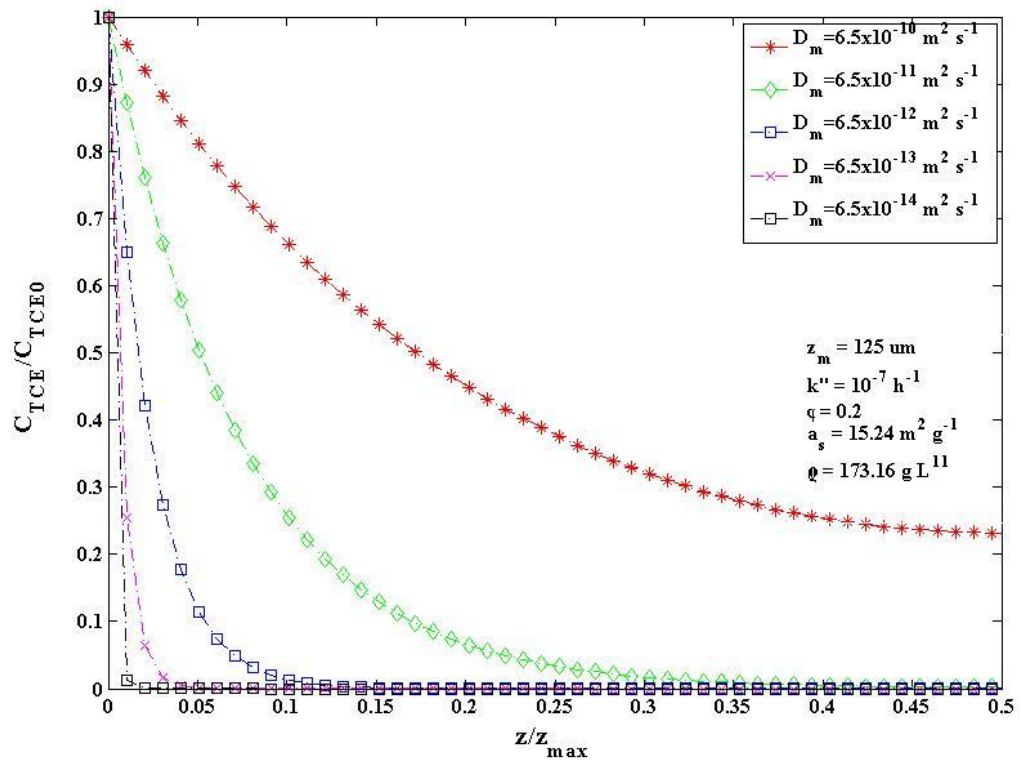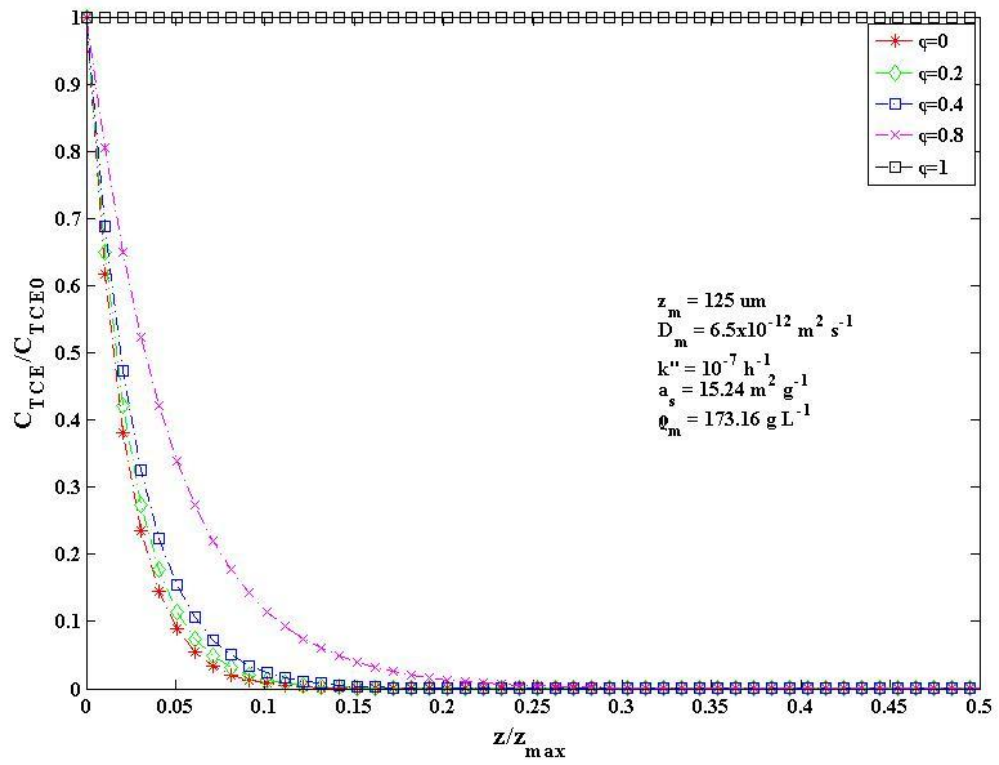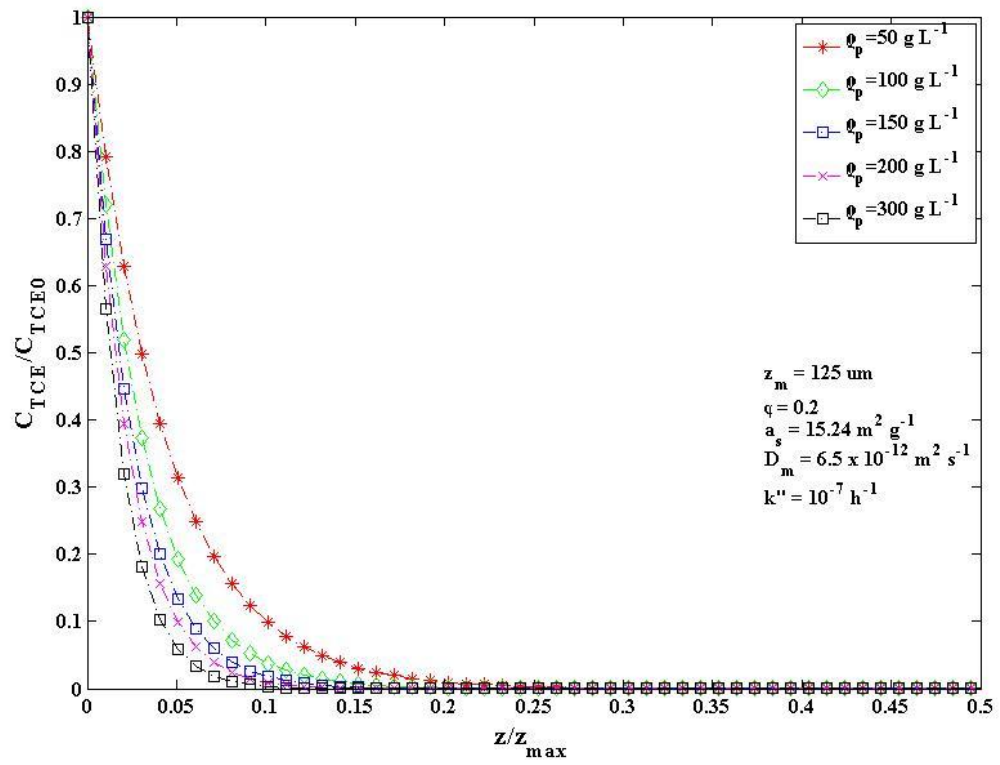
Figure 6.21 Plot of equation E5.4 describing TCE concentration change within Fe/Pd functionalized PAA/PVDF membrane at different mass concentration ρ_m with constant φ, k'', a_s and D_m.

6.5.2 Validation with experiment data

Reaction rate of TCE dechlorination is the function of NPs surface area a_s, NPs mass concentration in membrane ρ_m (ranging for 0.3 g L^{-1} to 4.4 g L^{-1} based on membrane pore volume and Pd NPs loading) and surface-area-based rate constant k'' from E5.3 (assuming void volume φ is 0.2). Surface-area-based rate constant k'' describes reductive reaction on Fe/Pd NPs. Reaction environment (in membrane or in solution) has no effect on k'' since surface-area-based rate is normalized. Therefore, in this study, k_{SA} obtained from experiment by using Fe/Pd NPs functionalized PAA/PVDF membranes could substitute k'' in equation E5.3 to calculate Thiele modules. Values of corresponding Thiele modules and effectiveness factors at different experiment conditions were given in Table 6.1. The value of Thiele modules Φ indicated that this membrane system is diffusion limiting as expected, since no internal mixing provided in membrane pores. However, effectiveness factor η implied that reaction rate in membrane was up to two magnitudes than that in bulk solution, i.e. k_{obs}. This indicates that membrane pores embedded with Fe/Pd NPs is a highly reductive environment that is favorable for TCE dechlorination.

Also, TCE dechlorination profile is investigated as shown in Figure 6.22 by assuming 0.2 void volume fraction. TCE was completely dechlorinated at 6% to 40% length of thickness. The result indicated that not all NPs in membrane pores participate in dechlorination experiment, and the actual reaction rate was much higher than what was observed. Therefore, k_{obs} needed modification since assumption that all NPs in membrane participated in reduction reaction was made, and this assumption was accepted by reported literatures (Xu et al., 2005; Xu and Bhattacharyya, 2007; Smuleac et al., 2010).

pH effect, metal loadings also showed impact on TCE dechlorination profile, it is expected since the concentration change in solution was observed in Figure 6.8 (different pH) and Figure 6.14 (different Pd loading). With lower loading of Pd NPs, higher pH, one could expect more NPs in membrane pores are utilized.

In this validation, k_{obs} in TCE dechlorination experiment using functionalized PAA/PVDF membrane was utilized to calculate and k'' in equation E6.1 and E5.3. However, more accurate results should be obtained by using the intrinsic reaction rate constant k_{int} to calculate k'' in order to perform membrane's efficiency. For example, k_{SA} from experiment using CMC-stabilized Fe/Pd NPs was considered to perform the intrinsic surface-area-normalized reaction rate constant, which was 1.061 L m^{-2} h^{-1} at pH 6.4 with 0.25 g L^{-1} Fe loading and 5 wt% Pd loading. The reaction rate constant in membrane k_m was calculated to be 56 h^{-1} (comparing 32.5 h^{-1} in membrane system), Φ and η were respectively 367 and 0.0027 (comparing 280 and 0.0036 in membrane system). This result showed higher value in Thiele modulus, which indicated membrane's diffusion limiting, and it also indicated that it was favorable for TCE dechlorination in membrane.

This modeling result applying experimental data showed that Fe/Pd NPs functionalized membranes are highly reductive system for TCE dechlorination. Thiele modulus indicated the system is diffusion limiting; therefore, TCE was completely dechlorinated before penetrated through membrane, causing low efficiency of functionalized membranes. However, by applying pressure (convective flow), increasing

diffusivity, this highly reductive system might be fully used in TCE dechlorination.

Reducing membrane thickness could also be a practical approach.

Table 6.1 Corresponding values of Thiele modulus and effectiveness factor based on k_m and k_{SA} at different pH and metal loading.

	Fe*, mg	Pd*, mg	pH	k_{obs}, h^{-1}	k_{SA}, L h^{-1} m^{-2}	k_m, h^{-1}	Φ	η
	10	0.5	6.4	2.346	0.616	32.50	280	0.0036
Fe/Pd functionalized	10	0.5	7.5	0.827	0.217	11.46	166	0.0060
PAA/PVDF membrane	10	0.5	9.6	0.459	0.120	6.36	124	0.0081
(40ml 30 ppm TCE solution)	4.56	0.04	6.4	0.181	0.104	0.44	33	0.0308
	17.28	0.2	6.4	1.851	0.281	5.94	119	0.0084

* Fe and Pd loading based on PAA/PVDF membrane with 13.2 cm^2 external area, 125 μm thickness and 70% porosity.

All experimental data calculated base on $a_s = 15.24$ m^2 g^{-1} and $D_m = 6.84 \times 10^{-12}$ m^2 s^{-1}.
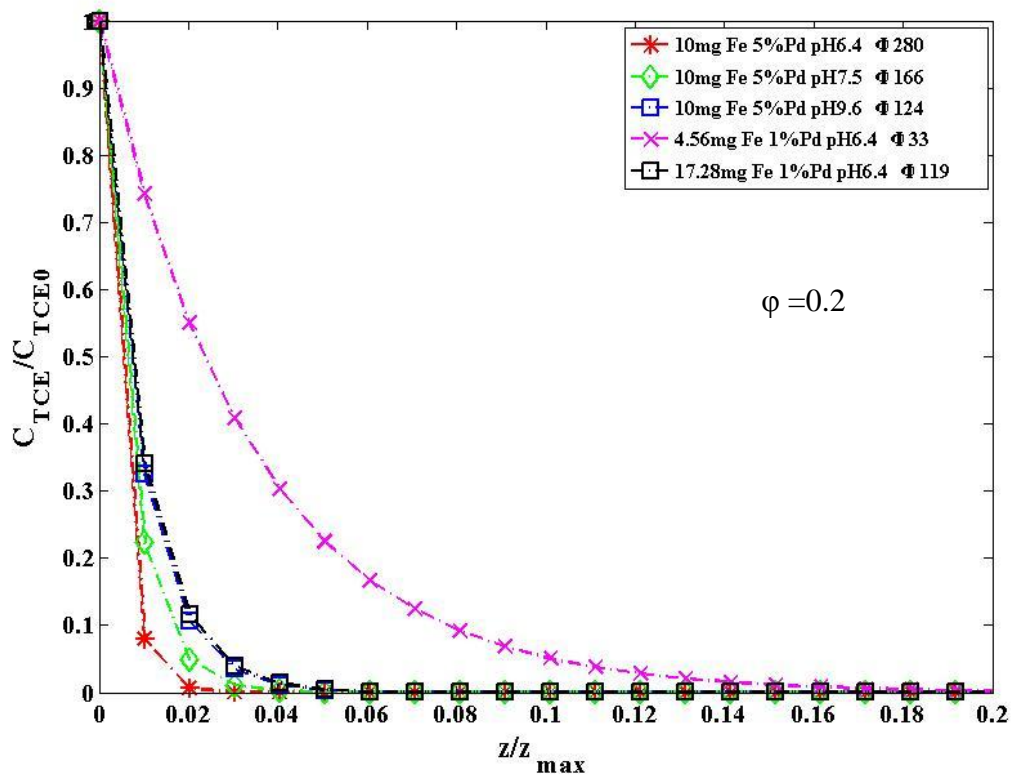
Figure 6.22 Plot of equation E5.4 describing TCE dechlorination profile by applying dechlorination experiment data using Fe/Pd NPs functionalized PAA/PVDF membranes. (feed solution: 40 ml 30 mg L^{-1} TCE, membrane external area: 13.2 cm^2, thickness: 125 μm)

6.5.3 TCE dechlorination considering adsorption and desorption

To discuss the relation between TCE concentration on NPs surface and in the bulk solution, TCE adsorption experiment was conducted to observe adsorption behavior on PAA/PVDF membranes and deactivated Fe/Pd functionalized membranes. At high value of TCE concentration, Figure 6.23 showed that it was Langmuir-type isotherm adsorption for this system. This result showed an agreement with open literature(Burris et al., 1995)(Tee et al., 2009). Therefore, the following expression could be used to describe the relation of TCE concentration on NPs surface and in the bulk solution:

$$q_{TCE} = Q\frac{KC_{TCE}}{1 + KC_{TCE}}$$
(E6.4)

where K is sorption parameter (L mmole^{-1}) and Q is the maximum adsorption concentration on the Fe/Pd functionalized PAA/PVDF membranes (mmole g^{-1}), respectively 2.2276 L mmole^{-1} and 0.0065 mmole g^{-1} obtained by using *nlinfit* command in MATLAB. In Figure 6.23, it also showed the comparison with TCE adsorption by PAA/PVDF membranes, for which K and Q are respectively 1.2747 L mmole^{-1} and 0.0051 mmole g^{-1}. In the functionalized membranes, PAA domain with crosslinking has hydrophobic sites that could attract TCE molecules, enhancing its concentration in PAA domain. For conveniences, it was assumed that all TCE were adsorbed by Fe/Pd in PAA domain in this study.

At low TCE concentration, the relation could be expressed by the following expression:

$$q_{TCE} = K_1 C_{TCE}$$
(E6.5)

where K_1 is the adsorption constant at C_{TCE} ranging from 0 mg L^{-1} to 30 mg L^{-1}, 0.0107 L g^{-1} for Fe/Pd functionalized membranes and 0.0055 L g^{-1} for PAA/PVDF membranes in Figure 6.23.

After combing equation (E5.18), (E6.4) and (E6.5), the final expression for concentration of TCE with time is:

At higher C_{TCE} (30 mg L^{-1} < C_{TCE}):

$$\frac{dC_{TCE}}{dt} = -K_A\left(1 + KC_{TCE}\right)C_{TCE} + \frac{VdK_B}{m_{Fe/Pd}KQ}\left(1 + KC_{TCE}\right)^2 C_{TCE} \tag{E6.6}$$

At lower C_{TCE} (0 mg L^{-1} < C_{TCE} < 30 mg L^{-1}):

$$\frac{dC_{TCE}}{dt} = -\left(K_A - \frac{VdK_B}{m_{Fe/Pd}K_1}\right)C_{TCE} \tag{E6.7}$$

Equation (E6.6) and (E6.7) describe the TCE degradation with time at different concentration ranges with adsorption assumption. At lower C_{TCE}, it is obvious that TCE degradation follows first-order dechlorination that is in an agreement in reported articles (Johnson et al., 1996)(Scherer et al., 1997). At higher C_{TCE}, equation (E6.6) indicates higher order of TCE dechlorination might be used to better describe the reaction mechanism.

However, in this study, most of the experiment data was obtain by applying 30 mg L^{-1} as initial C_{TCE}. Therefore, first-order dechlorination was proved to be accepted by both model and experiment in this study. In later study, investigation of k_{int} in TCE dechlorination and adsorption-desorption behavior should be necessarily discussed due to

its important role in the model to simulate the experiment data with higher TCE

concentration.
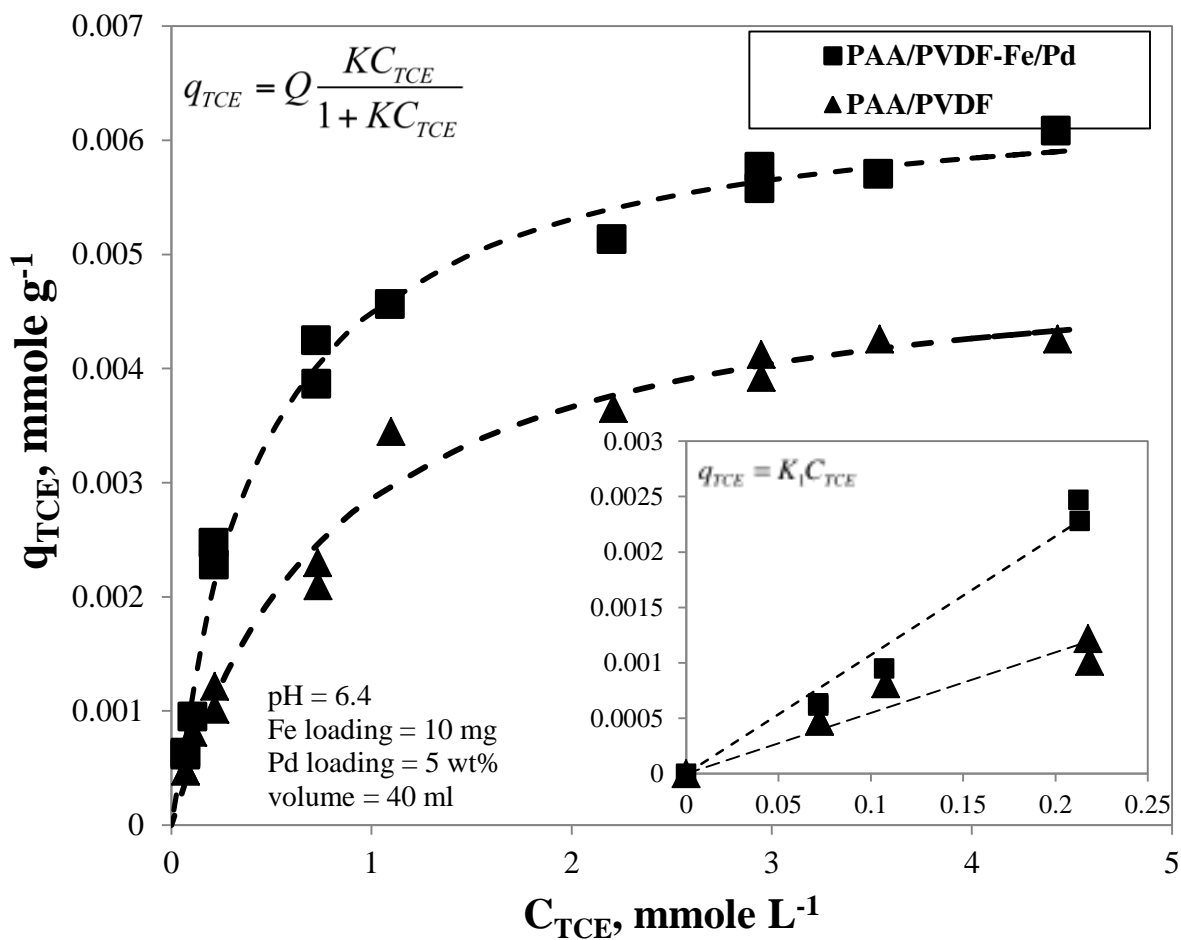
Figure 6.23 Langmuir isotherm for TCE dechlorination experiment in batch reaction by using deactivated Fe/Pd(5%) functionalized PAA/PVDF s and PAA/PVDF membranes at pH 6.4. Fe loading: 0.25 g L^{-1}. (Membrane external area: 13.2 cm^2)

Chaper 7   Conclusion

In this paper, cross-linked PAA functionalized PVDF membranes was synthesized by in-situ polymerization of acrylic acid. Fe NPs were successfully immobilized on the surface and inside PAA/PVDF membranes by ion exchange. Pd NPs was synthesized by dip coating. TCE chlorination was achieved at different metal loading (mostly with 1 wt% or 5 wt% Pd) and different pH values (ranging from 4 to 10) by using CMC stabilization and PAA/PVDF membrane synthesis. With higher Pd loading and lower pH value, more TCE was degraded to form Cl^- in both treatments. Comparing to CMC stabilized Fe/Pd NPs system, PAA/PVDF membranes not only prevent the aggregation of NPs, but also reduce the lost of NPs during the process of recapture of NPs by adding reductive agent.

Thiele modulus was introduced to discuss the TCE dechlorination profile in membrane pores by applying pseudo first-order kinetic, it was found that TCE dechlorination profile depended on several parameters including diffusivity, nanoparticle mass concentration, nanoparticle surface area, surface-based reaction rate and void volume fraction. TCE dechlorination profile was observed by changing specific parameter while changing others. Modeling results indicated that membrane pores embedded with Fe/Pd NPs is a highly reductive environment and only part of NPs embedded in membrane pores were utilized in TCE dechlorination in membrane system. It is proposed that modification is needed to correct the reaction rate observed in bulk solution. In addition TCE adsorption experiment was conducted to prove that Langmuir-type isotherm adsorption was suitable for this membrane system. This reduction mechanism considering adsorption and desorption on the surface of Fe/Pd functionalized

PAA/PVDF membranes could be used to discuss TCE dechlorination with high TCE concentration.

Nomenclature

k_{obs} = observed reaction rate constant (h^{-1})

k_m = reaction rate constant in membrane (h^{-1})

k_{SA}, k'' = surface reaction rate constant ($L\ m^{-2}\ s^{-1}$)

k_{int} = intrinsic reaction rate constant (h^{-1})

k_{ad} = adsorption reaction rate constant (h^{-1})

k_{-ad} = reverse adsorption reaction rate constant (h^{-1})

C_A, C_{TCE} = TCE concentration in solution ($mg\ L^{-1}$)

C_{A0}, C_{TCE0} = initial TCE concentration in solution ($mg\ L^{-1}$)

C_F = TCE concentration in feed side compartment ($mg\ L^{-1}$)

C_P = TCE concentration in permeate side compartment ($mg\ L^{-1}$)

L = membrane thickness (m)

A = permeate membrane area (m^2)

V_c = the volume of the compartments of both feed and permeate side (m^3)

t = permeate time (s)

H = TCE partitioning coefficient through membrane

D_m = TCE diffusivity through the membrane ($m^2\ s^{-1}$)

E = voltage signal detected by chloride electrode (mV)

a, b = constants in Nernst equation to calculate chloride concentration

z = axial direction of membrane (m)

r_A = rate of generation of TCE per volume, (mmole s^{-1} L^{-1})

a_s = surface area of the NPs (m^2 g^{-1})

d_p = iron/palladium nanopartical diameter (nm)

z = axial coordinates (m)

z' = dimensionless axial coordinate

C' = dimensionless TCE concentration

S = active sites on nanoparticles surface

V = volume of feed solution (L)

$m_{Fe/Pd}$ = bimetallic loading (mg)

q_{TCE} = TCE concentration in membrane domain (mmole g^{-1})

K = sorption parameter (L mmole^{-1})

K_1 = sorption constant

Q = maximum adsorption concentration on the Fe/Pd functionalized PAA/PVDF

membranes (mmole g^{-1})

Greek letters

φ = void volume fraction

ρ_m = mass concentration of the NPs (g L^{-1})

δ = percentage of active sites on NPs surface

Φ = Thiele modulus

η = effectiveness factor

Chemical / polymer symbols

PAA: Poly acrylic acid

PVDF: Polyvinylidene fluoride

TCE: Trichloroethylene

CMC: Carboxymethyl cellulose

References

Ahn, J., Chung, W.-J., Pinnau, I., and Guiver, M.D. (2008). Polysulfone/silica nanoparticle mixed-matrix membranes for gas separation. Journal of Membrane Science *314*, 123–133.

Amendola, V., Meneghetti, M., Granozzi, G., Agnoli, S., Polizzi, S., Riello, P., Boscaini, A., Anselmi, C., Fracasso, G., Colombatti, M., et al. (2011). Top-down synthesis of multifunctional iron oxide nanoparticles for macrophage labelling and manipulation. Journal of Materials Chemistry *21*, 3803.

Andersin, J., Parkkinen, P., and Honkala, K. (2012). Pd-catalyzed hydrodehalogenation of chlorinated olefins: Theoretical insights to the reaction mechanism. Journal of Catalysis *290*, 118–125.

Behari, J. (2010). Principles of nanoscience: an overview. Indian J. Exp. Biol. *48*, 1008–1019.

Bhattacharyya, D., Hestekin, J.., Brushaber, P., Cullen, L., Bachas, L.., and Sikdar, S.. (1998). Novel poly-glutamic acid functionalized microfiltration membranes for sorption of heavy metals at high capacity. Journal of Membrane Science *141*, 121–135.

Boal, A.K., Ilhan, F., DeRouchey, J.E., Thurn-Albrecht, T., Russell, T.P., and Rotello, V.M. (2000). Self-assembly of nanoparticles into structured spherical and network aggregates. Nature *404*, 746–748.

Burris, D.R., Campbell, T.J., and Manoranjan, V.S. (1995). Sorption of Trichloroethylene and Tetrachloroethylene in a Batch Reactive Metallic Iron-Water System. Environ. Sci. Technol. *29*, 2850–2855.

Cao, X., Ma, J., Shi, X., and Ren, Z. (2006). Effect of TiO2 nanoparticle size on the performance of PVDF membrane. Applied Surface Science *253*, 2003–2010.

Chen, D.-H., and He, X.-R. (2001). Synthesis of nickel ferrite nanoparticles by sol-gel method. Materials Research Bulletin *36*, 1369–1377.

Chen, J.L., Al-Abed, S.R., Ryan, J.A., and Li, Z. (2001). Effects of pH on dechlorination of trichloroethylene by zero-valent iron. J. Hazard. Mater. *83*, 243–254.

Cwiertny, D.M., Bransfield, S.J., Livi, K.J.T., Fairbrother, D.H., and Roberts, A.L. (2006). Exploring the Influence of Granular Iron Additives on 1,1,1-Trichloroethane Reduction. Environ. Sci. Technol. *40*, 6837–6843.

Datta, S., Cecil, C., and Bhattacharyya, D. (2008). Functionalized Membranes by Layer-By-Layer Assembly of Polyelectrolytes and In Situ Polymerization of Acrylic Acid for Applications in Enzymatic Catalysis. Ind. Eng. Chem. Res. *47*, 4586–4597.

Durrer, L., Helbling, T., Zenger, C., Jungen, A., Stampfer, C., and Hierold, C. (2008). SWNT growth by CVD on Ferritin-based iron catalyst nanoparticles towards CNT sensors. Sensors and Actuators B: Chemical *132*, 485–490.

Geismann, C., and Ulbricht, M. (2005). Photoreactive Functionalization of Poly(ethylene terephthalate) Track-Etched Pore Surfaces with "Smart" Polymer Systems. Macromolecular Chemistry and Physics *206*, 268–281.

Glavee, G.N., Klabunde, K.J., Sorensen, C.M., and Hadjipanayis, G.C. (1995). Chemistry of Borohydride Reduction of Iron(II) and Iron(III) Ions in Aqueous and Nonaqueous Media. Formation of Nanoscale Fe, FeB, and Fe2B Powders. Inorg. Chem. *34*, 28–35.

Grzelczak, M., Vermant, J., Furst, E.M., and Liz-Marzán, L.M. (2010). Directed Self-Assembly of Nanoparticles. ACS Nano *4*, 3591–3605.

Gui, M., Smuleac, V., Ormsbee, L., Sedlak, D., and Bhattacharyya, D. (2012). Iron oxide nanoparticle synthesis in aqueous and membrane systems for oxidative degradation of trichloroethylene from water. Journal of Nanoparticle Research *14*, 1–16.

Hara, J., Ito, H., Suto, K., Inoue, C., and Chida, T. (2005). Kinetics of trichloroethene dechlorination with iron powder. Water Research *39*, 1165–1173.

He, F., and Zhao, D. (2005). Preparation and Characterization of a New Class of Starch-Stabilized Bimetallic Nanoparticles for Degradation of Chlorinated Hydrocarbons in Water. Environ. Sci. Technol. *39*, 3314–3320.

He, F., and Zhao, D. (2008). Hydrodechlorination of trichloroethene using stabilized Fe-Pd nanoparticles: Reaction mechanism and effects of stabilizers, catalysts and reaction conditions. Applied Catalysis B: Environmental *84*, 533–540.

He, F., Zhao, D., Liu, J., and Roberts, C.B. (2007). Stabilization of Fe−Pd Nanoparticles with Sodium Carboxymethyl Cellulose for Enhanced Transport and Dechlorination of Trichloroethylene in Soil and Groundwater. Ind. Eng. Chem. Res. *46*, 29–34.

He, Y.Q., Chen, H.B., Sun, H., Wang, X.D., and Gao, J.P. (2012). A pH and Electric Responsive Graphene Oxide Based Composite Hydrogel. Advanced Materials Research *430-432*, 327–330.

Hota, G., Kumar, B., Ng, W., and Ramakrishna, S. (2008). Fabrication and characterization of a boehmite nanoparticle impregnated electrospun fiber membrane for removal of metal ions. Journal of Materials Science *43*, 212–217.

Hu, X., Cong, H., Shen, Y., and Radosz, M. (2007). Nanocomposite Membranes for CO2 Separations: Silica/Brominated Poly(phenylene oxide). Ind. Eng. Chem. Res. *46*, 1547–1551.

Huh, K., Kang, H., Lee, Y., and Bae, Y. (2012). pH-sensitive polymers for drug delivery. Macromolecular Research *20*, 224–233.

Järvinen, K., Åkerman, S., Svarfvar, B., Tarvainen, T., Viinikka, P., and Paronen, P. (1998). Drug Release from pH and Ionic Strength Responsive Poly(acrylic acid) Grafted Poly(vinylidenefluoride) Membrane Bags In Vitro. Pharmaceutical Research *15*, 802–805.

Jin, X., and Hsieh, Y.-L. (2005). pH-responsive swelling behavior of poly(vinyl alcohol)/poly(acrylic acid) bi-component fibrous hydrogel membranes. Polymer *46*, 5149–5160.

Johnson, T.L., Scherer, M.M., and Tratnyek, P.G. (1996). Kinetics of Halogenated Organic Compound Degradation by Iron Metal. Environ. Sci. Technol. *30*, 2634–2640.

Jung, M., Yong Eun, K., Lee, J.-K., Baik, Y.-J., Lee, K.-R., and Wan Park, J. (2001). Growth of carbon nanotubes by chemical vapor deposition. Diamond and Related Materials *10*, 1235–1240.

Lewis, S., Lynch, A., Bachas, L., Hampson, S., Ormsbee, L., and Bhattacharyya, D. (2009a). Chelate-Modified Fenton Reaction for the Degradation of Trichloroethylene in Aqueous and Two-Phase Systems. Environmental Engineering Science *26*, 849–859.

Lewis, S., Smuleac, V., Montague, A., Bachas, L., and Bhattacharyya, D. (2009b). Iron-Functionalized Membranes for Nanoparticle Synthesis and Reactions. Separation Science and Technology *44*, 3289–3311.

Li, L., Abe, Y., Kanagawa, K., Shoji, T., Mashino, T., Mochizuki, M., Tanaka, M., and Miyata, N. (2007). Iron-chelating agents never suppress Fenton reaction but participate in quenching spin-trapped radicals. Analytica Chimica Acta *599*, 315–319.

Li, S., Fang, Y.-L., Romanczuk, C.D., Jin, Z., Li, T., and Wong, M.S. (2012). Establishing the trichloroethene dechlorination rates of palladium-based catalysts and iron-based reductants. Applied Catalysis B: Environmental *125*, 95–102.

Li, Y., Kim, W., Zhang, Y., Rolandi, M., Wang, D., and Dai, H. (2001). Growth of Single-Walled Carbon Nanotubes from Discrete Catalytic Nanoparticles of Various Sizes. J. Phys. Chem. B *105*, 11424–11431.

Lin, S.-S., and Gurol, M.D. (1998). Catalytic Decomposition of Hydrogen Peroxide on Iron Oxide: Kinetics, Mechanism, and Implications. Environ. Sci. Technol. *32*, 1417–1423.

Liu, Y., and Lowry, G.V. (2006). Effect of Particle Age (Fe0 Content) and Solution pH On NZVI Reactivity: H2 Evolution and TCE Dechlorination. Environ. Sci. Technol. *40*, 6085–6090.

Liu, Y., Majetich, S.A., Tilton, R.D., Sholl, D.S., and Lowry, G.V. (2005). TCE dechlorination rates, pathways, and efficiency of nanoscale iron particles with different properties. Environ. Sci. Technol. *39*, 1338–1345.

Lu, A.-H., Salabas, E.L., and Schüth, F. (2007). Magnetic nanoparticles: synthesis, protection, functionalization, and application. Angew. Chem. Int. Ed. Engl. *46*, 1222–1244.

Lu, Y., Yin, Y., Mayers, B.T., and Xia, Y. (2002). Modifying the Surface Properties of Superparamagnetic Iron Oxide Nanoparticles through A Sol−Gel Approach. Nano Lett. *2*, 183–186.

Mackenzie, K., Bleyl, S., Georgi, A., and Kopinke, F.-D. (2012). Carbo-Iron – An Fe/AC composite – As alternative to nano-iron for groundwater treatment. Water Research *46*, 3817–3826.

Nutt, M.O., Heck, K.N., Alvarez, P., and Wong, M.S. (2006). Improved Pd-on-Au bimetallic nanoparticle catalysts for aqueous-phase trichloroethene hydrodechlorination. Applied Catalysis B: Environmental *69*, 115–125.

Pignatello, J.J., Oliveros, E., and MacKay, A. (2006). Advanced Oxidation Processes for Organic Contaminant Destruction Based on the Fenton Reaction and Related Chemistry. Critical Reviews in Environmental Science and Technology *36*, 1–84.

Qiang, Z., Ben, W., and Huang, C.-P. (2008). Fenton process for degradation of selected chlorinated aliphatic hydrocarbons exemplified by trichloroethylene, 1,1-dichloroethylene and chloroform. Frontiers of Environmental Science & Engineering in China *2*, 397–409.

Ried, A., and Krüger, J. (2009). Which Advanced Oxidation Process is Best? An Effective Method for Micropollutant Removal in Contaminated Groundwater. Proceedings of the Water Environment Federation *2009*, 476–484.

Roberts, A.L., Totten, L.A., Arnold, W.A. [Johns H.U., Burris, D.R. [Armstrong L., and Campbell, T.J. [Applied R.A. (1996). Reductive elimination of chlorinated ethylenes by zero-valent metals.

Ruhl, A.S., Ünal, N., and Jekel, M. (2012). Evaluation of two-component Fe(0) fixed bed filters with porous materials for reductive dechlorination. Chemical Engineering Journal *209*, 401–406.

Scherer, M.M., Westall, J.C., Ziomek-Moroz, M., and Tratnyek, P.G. (1997). Kinetics of Carbon Tetrachloride Reduction at an Oxide-Free Iron Electrode. Environ. Sci. Technol. *31*, 2385–2391.

Seol, S.K., Kim, D., Jung, S., and Hwu, Y. (2011). Microwave synthesis of gold nanoparticles: Effect of applied microwave power and solution pH. Materials Chemistry and Physics *131*, 331–335.

Smidt, H., and de Vos, W.M. (2004). Anaerobic Microbial Dehalogenation. Annual Review of Microbiology *58*, 43–73.

Smuleac, V., Bachas, L., and Bhattacharyya, D. (2010). Aqueous − Phase Synthesis of PAA in PVDF Membrane Pores for Nanoparticle Synthesis and Dichlorobiphenyl Degradation. J Memb Sci *346*, 310–317.

Smuleac, V., Butterfield, D.A., and Bhattacharyya, D. (2006). Layer-by-layer-assembled microfiltration membranes for biomolecule immobilization and enzymatic catalysis. Langmuir *22*, 10118–10124.

Smuleac, V., Varma, R., Sikdar, S., and Bhattacharyya, D. (2011). Green Synthesis of Fe and Fe/Pd Bimetallic Nanoparticles in Membranes for Reductive Degradation of Chlorinated Organics. Journal of Membrane Science *379*, 131–137.

Su, Y., Hsu, C.-Y., and Shih, Y. (2012). Effects of various ions on the dechlorination kinetics of hexachlorobenzene by nanoscale zero-valent iron. Chemosphere *88*, 1346–1352.

Swift, D., Rothermel, J., Peterson, L., Orr, B., Bures, G.H., and Weidhaas, J. (2012). Remediating TCE-contaminated groundwater in low-permeability media using hydraulic fracturing to emplace zero-valent iron/organic carbon amendment. Remediation Journal *22*, 49–67.

Tartakovsky, B., Manuel, M.-F., and Guiot, S.R. (2003). Trichloroethylene Degradation in a Coupled Anaerobic/Aerobic Reactor Oxygenated Using Hydrogen Peroxide. Environ. Sci. Technol. *37*, 5823–5828.

Tee, Y.-H., Bachas, L., and Bhattacharyya, D. (2009). Degradation of Trichloroethylene by Iron-Based Bimetallic Nanoparticles. J. Phys. Chem. C *113*, 9454–9464.

Tratnyek, P.G., Johnson, T.L., Scherer, M.M., and Eykholt, G.R. (1997). Remediating Ground Water with Zero-Valent Metals: Chemical Considerations in Barrier Design. Ground Water Monitoring & Remediation *17*, 108–114.

Tyre, B.W., Watts, R.J., and Miller, G.C. (1991). Treatment of Four Biorefractory Contaminants in Soils Using Catalyzed Hydrogen Peroxide. Journal of Environmental Quality *20*, 832–838.

Ulbricht, M., and Yang, H. (2005). Porous Polypropylene Membranes with Different Carboxyl Polymer Brush Layers for Reversible Protein Binding via Surface-Initiated Graft Copolymerization. Chem. Mater. *17*, 2622–2631.

Wang, C.-B., and Zhang, W. (1997). Synthesizing Nanoscale Iron Particles for Rapid and Complete Dechlorination of TCE and PCBs. Environ. Sci. Technol. *31*, 2154–2156.

Wang, Q., Jeong, S.-W., and Choi, H. (2012). Removal of trichloroethylene DNAPL trapped in porous media using nanoscale zerovalent iron and bimetallic nanoparticles: Direct observation and quantification. Journal of Hazardous Materials *213–214*, 299–310.

Xia, D., Li, D., Ku, Z., Luo, Y., and Brueck, S.R.J. (2007). Top-down approaches to the formation of silica nanoparticle patterns. Langmuir *23*, 5377–5385.

Xu, J., and Bhattacharyya, D. (2007). Fe/Pd Nanoparticle Immobilization in Microfiltration Membrane Pores: Synthesis, Characterization, and Application in the Dechlorination of Polychlorinated Biphenyls. Ind. Eng. Chem. Res. *46*, 2348–2359.

Xu, J., and Bhattacharyya, D. (2008). Modeling of Fe/Pd Nanoparticle-Based Functionalized Membrane Reactor for PCB Dechlorination at Room Temperature. J. Phys. Chem. C *112*, 9133–9144.

Xu, J., Dozier, A., and Bhattacharyya, D. (2005). Synthesis of Nanoscale Bimetallic Particles in Polyelectrolyte Membrane Matrix for Reductive Transformation of Halogenated Organic Compounds. Journal of Nanoparticle Research *7*, 449–467.

Yeh, C.K.-J., Chen, W.-S., and Chen, W.-Y. (2004). Production of Hydroxyl Radicals from the Decomposition of Hydrogen Peroxide Catalyzed by Various Iron Oxides at pH 7. Practice Periodical of Hazardous, Toxic, and Radioactive Waste Management *8*, 161–165.

Zhang, W. (2003). Nanoscale Iron Particles for Environmental Remediation: An Overview. Journal of Nanoparticle Research *5*, 323–332.

Zhang, W., Li, L., Lin, K., Xiong, B., Li, B., Lu, S., Guo, M., and Cui, X. (2012). Synergetic degradation of Fe/Cu/C for groundwater polluted by trichloroethylene. Water Sci. Technol. *65*, 2258–2264.

Zhang, W., Wang, C.-B., and Lien, H.-L. (1998). Treatment of chlorinated organic contaminants with nanoscale bimetallic particles. Catalysis Today *40*, 387–395.

Zhao, Y., Newton, J.N., Liu, J., and Wei, A. (2009). Dithiocarbamate-Coated SERS Substrates: Sensitivity Gain by Partial Surface Passivation†. Langmuir *25*, 13833–13839.

Vita

The author, Ruo He, was born in Qionghai, Hainan province, China, in October 1987. She graduated from Tsinghua University with a Bachelor of Science degree in chemical engineering in 2010. She joined the master program in Chemical and Materials Engineering at the University of Kentucky, Lexington in Fall 2010.